Propositions

1. Two equally dense systems may have different total small-angle scattering cross sections depending on the mutual arrangement of particles.

2. The counterintuitive rule of thumb for anisotropic objects with a long and a short axis:
   long axis parallel to the beam: **more** scattering
   long axis perpendicular to the beam: **less** scattering.

3. Correlation functions can be defined *per (sub)system, per particle, per unit volume, with dimensionless variables, normalized* and combinations of those, which usually creates a mess in notations. Therefore it is best to leave those definitions up to the reader and stress the understanding of ideas.

4. Real space compared to reciprocal space techniques can not have neither advantages nor disadvantages. There are only bad and good applications.

5. SESANS is really a correlometer, rather than a diffractometer. [1]

6. The statement "SESANS measures interparticle interference more accurately than the form factor of an individual particle"[1] is not true.

7. Bilateral integration is not necessarily equal to two unilateral ones. It is untrue in odd cases. The same applies to social integration.

8. Wave interference does not necessarily produce a constructive effect. The same applies to interference of scientists.

9. Application of SESANS to lunar rocks and other fantastic objects may eventually attract a lot of money and the interest of laymen.

These propositions are considered opposable and defendable and as such have been approved by the supervisor, Prof. Dr. I.M. de Schepper.

---

[1] D.W. Schaefer & M.M. Agamalian, Curr.Opin.Sol.State and Mat.Sci. 8, (2004), 39-47

Stellingen

1. Twee systemen met gelijke dichtheid kunnen verschillende totale kleine hoek verstrooiingsdoorsnedes hebben, afhankelijke van de onderlinge rangschikking van de deeltjes.

2. De vuistregel voor anisotrope objecten met een korte en lange as gaat tegen het gevoel in:
   lange as parallel aan de bundel: **meer** verstrooiing
   lange as loodrecht op de bundel: **minder** verstrooiing.

3. Correlatiefuncties kunnen worden gedefinieërd *per (sub)systeem, per deeltje, per volume, met dimensieloze variabelen, genormaliseerd* en in combinaties hiervan, wat gewoonlijk een chaos in notaties genereert. Daarom is het beter deze definities aan de lezer over te laten en het begrip van de ideeën erachter te benadrukken.

4. Reeële ruimte- vergeleken met de reciproke ruimtetechnieken hebben geen voordelen of nadelen. Er zijn slechts goede en slechte toepassingen.

5. SESANS is eerder een correlometer, dan een diffractometer.[1]

6. De bewering: "SESANS meet veeleer de interferentie tussen deeltjes dan de vormfactor van een afzonderlijk deeltje"[1] is niet waar.

7. Tweezijdige integratie is niet noodzakelijkerwijs gelijk aan twee eenzijdige integraties. Hetzelfde geldt voor sociale integratie.

8. Interferentie van golven is niet noodzakelijkerwijs constructief. Hetzelfde geldt voor interferentie tussen wetenschappers.

9. Het toepassen van SESANS op maanstenen en dergelijke fantastische monsters kan op de lange duur de belangstelling van de leken opwekken en daarmee veel geld aantrekken.

Deze stellingen worden opponeerbaar en verdedigbaar geacht en zijn als zodanig goedgekeurd door de promotor, Prof. Dr. I.M. de Schepper.

---

[1]D.W. Schaefer & M.M. Agamalian, Curr. Op. Sol.State and Mat.Sci. 8, (2004), 39-47.

Spin-Echo Small-Angle Neutron Scattering applied to colloidal systems

Spin-Echo Small-Angle Neutron Scattering applied to colloidal systems

Timofey Vladislavovich KRUGLOV

master of science in physics
Saint-Petersburg State University, Russia
geboren te Narva, Estland

Dit proefschrift is goedgekeurd door de promotor:
Prof. dr. I.M. de Schepper

Toegevoegd promotor:
Dr. W.G. Bouwman

Samenstelling promotiecommissie:

Rector Magnificus	voorzitter
Prof. dr. I.M. de Schepper	Technische Universiteit Delft, promotor
Prof. dr. ir. C.W.E. van Eijk	Technische Universiteit Delft
Prof. dr. M.A. Cohen Stuart	Universiteit Wageningen
Prof. dr. S.W. de Leeuw	Technische Universiteit Delft
Dr. W.G. Bouwman	Technische Universiteit Delft, toegevoegd promotor
Dr. M.Th. Rekveldt	Technische Universiteit Delft
Dr. A.V. Petukhov	Universiteit Utrecht

Printed in the Netherlands

Contents

Statement of Purpose

A new technique has its value as long as it is known *what* is measures, not
only *how* it measures. Paradoxically the actual development [24, 26] and ap-
plication of SESANS [2] started before its measured quantities were fully inter-
preted. This thesis provides a manual on the methodology and interpretation
of the SESANS measurements. Chapter "Theory" could have been named
also "What SESANS actually measures". Chapter "Experiment" could have
been named "What SESANS is actually able to measure". The subject of this
thesis both theoretical and experimental is focused on isotropic particles (solid
spheres, shells and gaussian coils) and structures formed by spherical particles.

While developing my PhD project I kept in mind the following reasons to
pursue the case of spherical particles:

- A *biggest class* of colloidal systems is formed by spherical particles. Ster-
  ically stabilized (hard sphere) and charge stabilized colloids are most
  notorious of them. Plenty of well-characterized ones are avaliable [23].
  Those were naturally the first candidates to be probed with the new
  technique.

- It appeared to be possible (even though not easy) to handle *analytically*
  functions involved in a description of spherical particles (see chapters
  3,5 and 9). They can be found in the numerous appendices in this the-
  sis. These allow people who are not experts in numerical recipies and
  programming to use these functions with any fitting software.

- Spherical shapes (for particles themselves and for potentials) are good
  approximation in many cases where they are not exactly spherical (chap-
  ter 7). It is a matter of future development of SESANS interpretation
  methodology to find more advanced solutions.

- Many structures can very well be approximated by a set of spheres with
  special arrangement. This is known as the sphere subparticles method[6].

This approach is ready to be developed since all necessary correlation functions are presented in this thesis.

Additionally to the above reasons for applications of SESANS to colloids composed of spherical particles, there are also reasons why colloids in general are one of the best fit applications for SESANS:

- *Length scale.* Ranges from $10nm$ to $15\mu m$, which is essentially the same as the size range where the term *colloid* is defined.

- *Multiple scattering.* Colloids, especially concentrated ones, exhibit multiple scattering, which is extremely easy to handle in SESANS' real space domain (sec.1.3) compared to the reciprocal space of conventional scattering techniques.

- *Real space.* SESANS benefits from real space not only in terms of easy-to-handle-multiple-scattering. The interpretation in real space is much more straightforward, especially when the local structure is concerned (see part II).

Part I

Theory

Fourier Transform

Major parts of chapters 1 and 2 rely heavily on Fourier transform, so we precede those with a short summary of Fourier transform properties.

The normalization factors in Fourier transforms are based on the following integral:

$$\int_{-\infty}^{+\infty} e^{ikx}dx = 2\pi\delta(k) \tag{1}$$

If we define a Fourier images of a one dimensional function in a following way:

$$f(k) = \int_{-\infty}^{-\infty} e^{ikx}f(x)dx \tag{2}$$

$$f(x) = \frac{1}{2\pi}\int_{-\infty}^{+\infty} e^{-ikx}f(k)dk \tag{3}$$

By performing forth and back transforms of a function it is easy to show that this definition is normalized:

$$f(k) = \int_{-\infty}^{+\infty} e^{ikx}f(x)dx$$
$$= \frac{1}{2\pi}\int_{-\infty}^{+\infty} e^{ikx}\int_{-\infty}^{+\infty} e^{-ik'x}f(k')dk'dx$$
$$= \frac{1}{2\pi}\int_{-\infty}^{+\infty} f(k')dk'\int_{-\infty}^{+\infty} e^{i(k-k')x}dx$$
$$= \frac{1}{2\pi}\int_{-\infty}^{+\infty} f(k')dk'2\pi\delta(k-k')$$
$$= f(k)$$

In case of n-dimensional function it is obvious that the normalization is given by (each dimension gives a factor 2π (see (1)) upon forth and back transform):

$$f(\mathbf{q}) = \int_{-\infty}^{+\infty} e^{i\mathbf{qr}}f(\mathbf{r})d^n\mathbf{r} \tag{4}$$

$$f(\mathbf{r}) = \frac{1}{(2\pi)^n} \int_{-\infty}^{+\infty} e^{-i\mathbf{q}\mathbf{r}} f(\mathbf{q}) d^n \mathbf{q} \tag{5}$$

where $\mathbf{q}$ and $\mathbf{r}$ are n-dimensional vectors.

If $n = 2$ and $\mathbf{q} = (q_y, q_z)$ and $\mathbf{r} = (y, z)$ then

$$f(\mathbf{q}) = \int_{-\infty}^{+\infty} e^{i\mathbf{q}\mathbf{r}} f(\mathbf{r}) d^2 \mathbf{r} \tag{6}$$

$$f(\mathbf{r}) = \frac{1}{4\pi^2} \int_{-\infty}^{+\infty} e^{-i\mathbf{q}\mathbf{r}} f(\mathbf{q}) d^2 \mathbf{q} \tag{7}$$

or in case of isotropic functions in polar coordinates

$$f(q) = 2\pi \int_{-\infty}^{+\infty} \langle e^{i\mathbf{q}\mathbf{r}} \rangle f(r) r dr \tag{8}$$

$$f(r) = \frac{1}{2\pi} \int_{-\infty}^{+\infty} \langle e^{-i\mathbf{q}\mathbf{r}} \rangle f(q) q dq \tag{9}$$

where

$$\langle e^{i\mathbf{q}\mathbf{r}} \rangle = \frac{1}{2\pi} \int_{0}^{2\pi} e^{iqr\cos\varphi} d\varphi = J_0(qr) \tag{10}$$

where $J_0(qr)$ is a Bessel function.

Thus the transforms will take the following form

$$f(q) = 2\pi \int_{-\infty}^{+\infty} J_0(qr) f(r) r dr \tag{11}$$

$$f(r) = \frac{1}{2\pi} \int_{-\infty}^{+\infty} J_0(qr) f(q) q dq \tag{12}$$

better known as Hankel transform. It is normalized as well.

Chapter 1

Scattering in real space

SESANS being a real space scattering technique relies on the real space description of the scattering media in terms of correlation function. Conventional scattering techniques operate in the reciprocal space, where the scattering cross section is measured. This chapter provides the connection between these two spaces in the most general case.

1.1 Reciprocal versus real space

Let V is the volume of the sample illuminated by the neutron beam. The sample is described by the spatial distribution of the scattering length density $\rho(\mathbf{r})$. The scattering takes place on the scattering length density difference or *contrast*

$$\Delta\rho(\mathbf{r}) = \rho(\mathbf{r}) - \langle\rho\rangle$$

The amplitude of elastic neutron scattering $F(\mathbf{q})$ of such a sample is:

$$F(\mathbf{q}) = \int_V d\mathbf{r}\, e^{i\mathbf{q}\mathbf{r}} \Delta\rho(\mathbf{r}) \tag{1.1}$$

The differential scattering cross section of the sample is then expressed as:

$$\frac{d\Sigma(\mathbf{q})}{d\Omega} = F(\mathbf{q})F^*(\mathbf{q}) = \int_V d\mathbf{r}' \int_V d\mathbf{r}''\, e^{-i\mathbf{q}(\mathbf{r}'-\mathbf{r}'')} \Delta\rho(\mathbf{r}')\Delta\rho(\mathbf{r}'') \tag{1.2}$$

If we define the vector:

$$\mathbf{r} = \mathbf{r}' - \mathbf{r}'' \tag{1.3}$$

we can rewrite (1.2) as:

$$\frac{d\Sigma(\mathbf{q})}{d\Omega} = \int_V d\mathbf{r} e^{-i\mathbf{qr}} \int_V d\mathbf{r}' \Delta\rho(\mathbf{r} + \mathbf{r}')\Delta\rho(\mathbf{r}') \tag{1.4}$$

The correlation function of a sample defined as [32]:

$$\gamma(\mathbf{r}) = \int_V d\mathbf{r}' \Delta\rho(\mathbf{r}')\Delta\rho(\mathbf{r}' + \mathbf{r}) \tag{1.5}$$

so we can rewrite (1.4) as:

$$\frac{d\Sigma(\mathbf{q})}{d\Omega} = \int_V d\mathbf{r} e^{-i\mathbf{qr}} \gamma(\mathbf{r}) \tag{1.6}$$

1.2   Small-angle approximation in real space

Let x-axis be the direction of the neutron beam and S is the beam cross section. In the small angle approximation we put the component of a scattering vector along the beam $q_x = 0$. Then a cumulative scattering probability of a sample would be

$$\frac{d\Sigma(0, q_y, q_z)}{Sd\Omega} = \frac{1}{S}\int_V dy dz e^{i(q_y y + q_z z)}\gamma(x, y, z)dx \tag{1.7}$$

Here we define a small-angle correlation function

$$G_c(y, z) = \frac{\lambda^2}{S}\int_{-\infty}^{+\infty}\gamma(x, y, z)dx \tag{1.8}$$

where λ is a neutron wavelength. It is a projection of the conventional c.f. along a neutron beam. Now (1.7) can be rewritten as

$$\frac{d\Sigma(q_y, q_z)}{Sd\Omega} = \frac{1}{\lambda^2}\int_{yz} dy dz e^{i(q_y y + q_z z)}G(y, z) \tag{1.9}$$

This is the cumulative differential scattering probability at the angle (q_y, q_z). The x-component is excluded from both sides, so we are dealing with two dimensional functions in the plane perpendicular to the beam. As can be immediately inferred from (1.9), $\frac{d\Sigma(q_y, q_z)}{Sd\Omega}$ and $G_c(y, z)$ are Fourier images of each other in yz-plane. Both functions are dimensionless.

1.3   Multiple scattering in real space

Following the approach taken in [27] we will distinguish *cumulative* [1] $\frac{d\Sigma(\mathbf{q})}{Sd\Omega}$ and *true* scattering probability $\frac{d\Sigma^*(\mathbf{q})}{Sd\Omega}$ which is actually observed for a sample with an arbitrary multiplicity of scattering.

It was shown that those two probabilities in a small-angle approximation are connected in a following way:

$$\frac{d\Sigma^*(\mathbf{q})}{Sd\Omega} = e^{-\frac{\Sigma}{S}} \sum_{n=1}^{\infty} \frac{k_0^{-2n+2}}{n!} \left[* \frac{d\Sigma(\mathbf{q})}{Sd\Omega} \right]^n \qquad (1.10)$$

where $\left[* \frac{d\Sigma(\mathbf{q})}{Sd\Omega} \right]^n$ stands for n-fold convolution of $\frac{d\Sigma(\mathbf{q})}{Sd\Omega}$.
According to (1.9)

$$G_c(y,z) = \frac{1}{k_0^2} \int_{q_y q_z} dq_y dq_z e^{-i(q_y y + q_z z)} \frac{d\Sigma(q_y, q_z)}{Sd\Omega} \qquad (1.11)$$

Let us define the quantity $G^*(y,z)$

$$G^*(y,z) = \frac{1}{k_0^2} \int_{q_y q_z} dq_y dq_z e^{-i(q_y y + q_z z)} \frac{d\Sigma^*(q_y, q_z)}{Sd\Omega} \qquad (1.12)$$

It was shown [27] that those quantities relate to each other as

$$G^*(y,z) = e^{G_c(y,z) - G_c(0,0)} - e^{-G_c(0,0)} \qquad (1.13)$$

where $G_c(0,0) = \frac{\Sigma}{S}$ is the total *cumulative* scattering probability, $e^{-G_c(0,0)}$ is the transmission and

$$G^*(0,0) = 1 - e^{-G_c(0,0)} \qquad (1.14)$$

is the total *true* scattering probability. In case of single scattering

$$G^*(y,z) = G_c(y,z)$$

If we had a hypothetic real-space small-angle scattering device it would have measured $G^*(y,z)$ instead of $\frac{d\Sigma^*(\mathbf{q})}{Sd\Omega}$.

---

[1] in [27] referred to as *apparent*

Chapter 2

SESANS

2.1 Concept and measured quantities

Here we give a brief overview of SESANS measured quantities and relate them to the ones introduced in the previous sections. In SESANS neutrons undergo Larmor precession in magnetic fields before and after scattering on a sample[26]. The final precession phase is different for neutrons scattered by different angles. As a result of this precession, the initially polarized neutron beam becomes depolarized. In general case (including multiple scattering) the polarization measured by SESANS is given by [25]:

$$P(z) = e^{G_c(z) - G_c(0)} \qquad (2.1)$$

where the SESANS correlation function is:

$$G_c(z) = \frac{1}{k_0^2} \int_{-\infty}^{+\infty} dq_y \int_{-\infty}^{+\infty} dq_z \frac{d\Sigma(\mathbf{q})}{S d\Omega} \cos(q_z z) \qquad (2.2)$$

with $\mathbf{q} = (0, q_y, q_z)$. Apparently this expression is a particular case of the generic small-angle correlation function given by (1.11) with $y = 0$. SESANS is a particular implementation of real-space small-angle scattering technique

measuring correlations only in one direction. Therefore the formalism from the previous sections is applicable to SESANS with $y = 0$. Apparently

$$G_c(0) = G_c(0,0) = \frac{\Sigma}{S} \tag{2.3}$$

gives the *total cumulative* scattering probability.

Now we relate $P(z)$ defined by (2.1) to the *true* scattering probability $G^*(y, z)$ defined by (1.12).

The quantity

$$P(\infty) = e^{-G_c(0)} = e^{-\frac{\Sigma}{S}} = T$$

represents the remaining fraction of polarization (transmission) and lies within the range $0 \geq T \geq 1$ for any Σ.

The *depolarization*

$$\Delta P(z) = P(z) - P(\infty) = G^*(0, z)$$

is the fraction of polarization that is lost due to scattering at a given z and is equal to the *true* scattering probability $G^*(0, z)$ as defined by (1.13).

$$\Delta P(0) = G^*(0,0) = 1 - e^{-G_c(0)} \tag{2.4}$$

is the *total true* scattering probability, which lies between 0 and 1 (compare to (1.14)). The *total cumulative* scattering probability can take any value.

The next step is to relate $G(z)$ to $\gamma(\mathbf{r})$. The simplest way is to put $y = 0$ in (1.8):

$$G_c(z) = \frac{\lambda^2}{S} \int_{-\infty}^{+\infty} dx \gamma(x, 0, z) \tag{2.5}$$

Otherwise it can be obtained by substituting (1.7) to (2.2) with subsequent elimination of reciprocal components [15]. This expression is the key which allows a direct real space interpretation of $G_c(z)$ in terms of conventional correlation function.

Switching from x and z to $r = \sqrt{x^2 + 0^2 + z^2}$ and z coordinates gives the explicit analytical expression:

$$G_c(z) = 2\frac{\lambda^2}{S} \int_z^{+\infty} dr \frac{\gamma(r)r}{\sqrt{r^2 - z^2}} \tag{2.6}$$

If we use dimensionless real and reciprocal space variables the above two equations cast into

$$G(z) = \int_{-\infty}^{+\infty} dx \gamma(x, 0, z) \tag{2.7}$$

$$G(z) = 2 \int_{z}^{+\infty} dr \frac{\gamma(r)r}{\sqrt{r^2 - z^2}} \tag{2.8}$$

This equation is of Abel type and can be resolved with respect to $\gamma(r)$ (see app.2.2.3):

$$\gamma(r) = \frac{1}{\pi} \frac{1}{r} \frac{d}{dr} \int_{r}^{+\infty} dz \frac{G(z)z}{\sqrt{z^2 - r^2}} \tag{2.9}$$

For an isotropic case (2.2) becomes

$$
\begin{aligned}
G_c(z) &= \frac{1}{k_0^2} \int_{-\infty}^{+\infty} dq_y \int_{-\infty}^{+\infty} dq_z \frac{d\Sigma(\mathbf{q})}{Sd\Omega} \cos(q_z z) \\
&= \frac{1}{k_0^2} \int_{-\infty}^{+\infty} q dq \frac{d\Sigma(q)}{Sd\Omega} \int_{0}^{2\pi} \cos(qz \cos\varphi) d\varphi \\
&= \frac{2\pi}{k_0^2} \int_{-\infty}^{+\infty} J_0(qz) q dq \frac{d\Sigma(q)}{Sd\Omega} \\
&= \frac{\lambda^2}{2\pi} \int_{-\infty}^{+\infty} J_0(qz) q dq \frac{d\Sigma(q)}{Sd\Omega}
\end{aligned}
$$

where $J_0(qz)$ is 0th-order Bessel function of the 1st kind. This transformation is better known as Hankel transform. It is symmetric making $G(z)$ and $\frac{d\Sigma(q)}{d\Omega}$ mutual Hankel images. The same holds for $\Delta P(z)$ and $\frac{d\Sigma^*(q)}{d\Omega}$.

2.2 Appendices

2.2.1 Direct reciprocal space elimination

This appendix shows how reciprocal space can be directly eliminated from the equation (2.2). Substituting (1.6) in (2.2) we get:

$$G_c(z') = \frac{1}{S} \int_V d\mathbf{r} \int_{-\infty}^{+\infty} \frac{dq_y}{k} \int_{-\infty}^{+\infty} \frac{dq_z}{k} e^{-i(\mathbf{q}\mathbf{r} - q_z z')} \gamma(\mathbf{r})$$

First, we decouple cartesian coordinates in the exponent:

$$G_c(z') = \frac{1}{S}\frac{1}{k^2}\int_V d\mathbf{r}\int_{-\infty}^{+\infty}dq_y\int_{-\infty}^{+\infty}dq_z e^{-i(q_x x+q_y y+q_z(z-z'))}\gamma(\mathbf{r})$$

Integration over q_z gives:

$$G_c(z') = \frac{1}{S}\frac{2\pi}{k^2}\int_V d\mathbf{r}\int_{-\infty}^{+\infty}dq_y e^{-i(q_x x+q_y y)}\delta(z-z')\gamma(\mathbf{r})$$

Integration over z gives:

$$G_c(z') = \frac{1}{S}\frac{2\pi}{k^2}\int_{-\infty}^{+\infty}dx\int_{-\infty}^{+\infty}dy\int_{-\infty}^{+\infty}dq_y e^{-i(q_x x+q_y y)}\gamma(x,y,z')$$

Now we can change z' back to z

$$G_c(z) = \frac{1}{S}\frac{2\pi}{k^2}\int_{-\infty}^{+\infty}dx\int_{-\infty}^{+\infty}dy\int_{-\infty}^{+\infty}dq_y e^{-i(q_x x+q_y y)}\gamma(x,y,z)$$

Integration over q_y gives:

$$G_c(z) = \frac{1}{S}\left(\frac{2\pi}{k}\right)^2\int_{-\infty}^{+\infty}dx\int_{-\infty}^{+\infty}dy e^{-iq_x x}\delta(y)\gamma(x,y,z)$$

Integration over y gives:

$$G_c(z) = \frac{\lambda^2}{S}\int_{-\infty}^{+\infty}dx e^{-iq_x x}\gamma(x,0,z)$$

Then we put $q_x = 0$:

$$G_c(z) = \frac{\lambda^2}{S}\int_{-\infty}^{+\infty}dx\gamma(x,0,z)$$

This shows that the SESANS correlation function is a 2D projection of correlation function.

2.2.2 Alternative representation of $G(z)$

This section shows that $G(z)$ being a 2D projection of $\gamma(r)$ can be alternatively presented as a convolution of 2D projection of scattering density.

According to (2.7) the SESANS correlation function can be represented as a 2D projection of the conventional correlation function:

$$G(z) = \int_{-\infty}^{+\infty} dx \gamma(x, 0, z) \tag{2.10}$$

where

$$\gamma(\mathbf{r}) = \int_V d\mathbf{r}' \rho(\mathbf{r})\rho(\mathbf{r} + \mathbf{r}') \tag{2.11}$$

where $\mathbf{r} = (x, y, z)$ and $\mathbf{r}' = (x', y', z')$.

Substitution of (2.11) in (2.10) gives:

$$G(z) = \int_{-\infty}^{+\infty} dx \int_{-\infty}^{+\infty} dx' \int_{-\infty}^{+\infty} dy' \int_{-\infty}^{+\infty} dz' \rho(\mathbf{r}')\rho(\mathbf{r}' + \mathbf{r}) \tag{2.12}$$

Returning from $\mathbf{r}$ and $\mathbf{r}'$ introduced by (1.3) back to $\mathbf{r}$ and $\mathbf{r}'$ we have:

$$\mathbf{r}'' = \mathbf{r}' + \mathbf{r} \tag{2.13}$$

Applying (2.13) to (2.12) we have:

$$G(z) = \int_{-\infty}^{+\infty} dx'' \int_{-\infty}^{+\infty} dx' \int_{-\infty}^{+\infty} dy' \int_{-\infty}^{+\infty} dz' \rho(\mathbf{r}')\rho(\mathbf{r}'')$$

After change of function arguments according to (1.3) we have:

$$G(z) = \int_{-\infty}^{+\infty} dy' \int_{-\infty}^{+\infty} dz' \int_{-\infty}^{+\infty} dx' \rho(\mathbf{r}') \int_{-\infty}^{+\infty} dx'' \rho(\mathbf{r}'') \tag{2.14}$$

Putting

$$\rho_{yz}(y, z) = \int_{-\infty}^{+\infty} dx \rho(x, y, z)$$

we can rewrite (2.14) as

$$G(z) = \int_{-\infty}^{+\infty} dy' \int_{-\infty}^{+\infty} dz' \rho_{yz}(y', z')\rho_{yz}(y'', z'') =$$
$$\int_{-\infty}^{+\infty} dy' \int_{-\infty}^{+\infty} dz' \rho_{yz}(y', z')\rho_{yz}(y' + y, z' + z)$$

which is a convolution of 2D projections of $\rho(\mathbf{r})$.

Equation 2.14 can also be represented as:

$$G(\mathbf{S}) = \int_s d\mathbf{s}\rho_s(\mathbf{s})\rho_s(\mathbf{s} + \mathbf{S}) \tag{2.15}$$

Putting $y = 0$ we get

$$G(z) = \int_{-\infty}^{+\infty} dy' \int_{-\infty}^{+\infty} dz' \rho_{yz}(y', z')\rho_{yz}(y', z' + z) \tag{2.16}$$

This shows that $G(z)$ can be equally presented either as a projection of correlation function given by(2.7) or a convolution of 2D projections of scattering densities given by (2.15).

2.2.3   From $G(z)$ back to $\gamma(r)$

This section solves the integral equation 2.8 with respect to $\gamma(r)$.

$$G(z) = 2 \int_z^D dr \frac{\gamma(r)r}{\sqrt{r^2 - z^2}}$$

The first step is to multiply both sides of the above equation above by

$$\frac{z}{\sqrt{z^2 - s^2}}$$

where s is an auxiliary variable, and integrate the product over z from s to D:

$$\int_s^D dz \frac{G(z)z}{\sqrt{z^2 - s^2}} = 2 \int_s^D dz \frac{z}{\sqrt{z^2 - s^2}} \int_z^D dr \frac{\gamma(r)r}{\sqrt{r^2 - z^2}}$$

Swapping integration order we have:

$$\int_s^D dz \frac{G(z)z}{\sqrt{z^2 - s^2}} = 2 \int_s^D dr\gamma(r)r dr \underbrace{\int_s^r dz \frac{z}{\sqrt{r^2 - z^2}\sqrt{z^2 - s^2}}}_{\frac{\pi}{2}}$$

$$\int_s^D dz \frac{G(z)z}{\sqrt{z^2 - s^2}} = \pi \int_s^D dr\gamma(r)r dr$$

Differentiation of both sides by $\frac{d}{ds}$ gives

$$\gamma(s) = \frac{1}{\pi s}\frac{d}{ds}\int_s^D dz\frac{G(z)z}{\sqrt{z^2 - s^2}}$$

Now we have formula that allows us to recalculate the SESANS correlation function into the conventional correlation function.

Chapter 3

Noninteracting particles

3.1 Integral parameters

3.1.1 Scattering length

Suppose we have a system of N paricles and each particle has a scattering
length

$$b = \int_V d\mathbf{r}\rho(\mathbf{r})$$

Equation (1.4) at $q = 0$ gives:

$$\left.\frac{d\Sigma(\mathbf{q})}{d\Omega}\right|_{q=0} = \int_V d^3\mathbf{r}\gamma(r) = Nb^2 \tag{3.1}$$

Now we want to express total scattering length in terms of $G(z)$. The right
hand side of (2.7) is integration along x axis. Our goal is to complement this
integration to get $\int_V d^3\mathbf{r}\gamma(R)$. Let us consider this projection as an integration
along the main axis, x, in cylindrical coordinate system (see fig.3.1.1).

In order to get the integral over a 3D volume we have to compliment the
integration along X axis by the integration over the cylindrical layer $2\pi z dz$ in
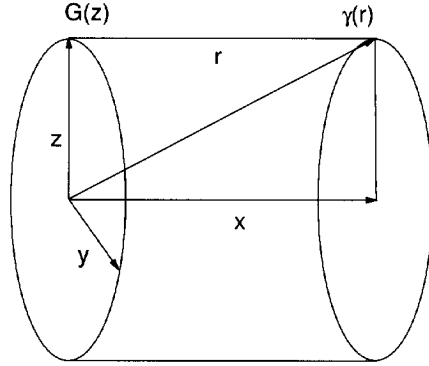both sides of (2.7)

Figure 3.1: Projection of 3D function $\gamma(r)$ along x-axis onto yz plane resulting in 2D function $G(y)$

$$2\pi \int_0^\infty G(z)z\,dz = \int_{-\infty}^{+\infty} dx \int_0^\infty 2\pi x\,dx\gamma(\sqrt{x^2 + 0^2 + x^2}) \qquad (3.2)$$

or

$$2\pi \int_0^\infty G(z)z\,dz = N \int_V \gamma(r)d\mathbf{r} = Nb^2 \qquad (3.3)$$

3.1.2   Guinier radius

The Guinier radius can be expressed via the distance distribution function:

$$R_g = \frac{\int_0^\infty p(r)r^2dr}{2\int_0^\infty p(r)dr} \qquad (3.4)$$

where:

$$p(r) = \gamma(r)r^2$$

First we recalculate denominator in terms of $G(z)$. Using

$$\int_V \gamma(r)d^3\mathbf{r} = \int_V \gamma(r)4\pi r^2 dr = 4\pi \int_V p(r)dr$$

equation (3.2) can be rewritten as:

$$\int_0^\infty G(z)z\,dz = 2\int_0^\infty p(r)\,dr$$

which is a normalization factor for distance distribution function.

We also need to recalculate the numerator of (3.4) in terms of $G(z)$ (see app.3.1.4):

$$\int_0^\infty p(r)r^2\,dr = \frac{3}{4}\int_0^\infty G(z)z^3\,dZ$$

and after normalization we have the Guinier radius expressed directly through $G(z)$:

$$R_g = \frac{3}{4}\frac{\int_0^\infty G(z)z^3\,dz}{\int_0^\infty G(z)z\,dz}$$

3.1.3   Total cumulative scattering cross section

$G_c(0)$ is a total cumulative scattering probability of a sample. Since particle are noninteraction for the whole sample it will be a sum of independent contibutions of N particles:

$$G_c(0) = \frac{\lambda^2}{S}NG(0) \tag{3.5}$$

It follows from (2.8) that:

$$G(0) = 2\int_0^\infty dr\gamma(r) \tag{3.6}$$

and

$$G_c(0) = 2\frac{\lambda^2}{S}N\int_0^\infty dr\gamma(r) \tag{3.7}$$

This value allows us to calculate the intensity of SESANS signal.

3.1.4   Appendix: Moments calculation

Equation (2.8) can be rewritten in terms of $p(r)$:

$$G(z) = 2 \int_z^\infty \frac{\gamma(r) r dr}{\sqrt{r^2 - z^2}} = 2 \int_z^\infty \frac{p(r) dr}{r\sqrt{r^2 - z^2}}$$

Using $< z^{n+1} > \propto < r^n >$ we multiply both sides of the equation on z^3 and integrate over dz:

$$\int_0^\infty G(z) z^3 dz = 2 \int_0^\infty z^3 dz \int_z^\infty \frac{p(r) dr}{r\sqrt{r^2 - z^2}}$$

After swap of integration order we have:

$$\int_0^\infty G(z) z^3 dz = 2 \int_0^\infty \frac{p(r) dr}{r} \int_0^r \frac{z^3 dz}{\sqrt{r^2 - z^2}}$$

Using:

$$\int_0^r \frac{z^3 dz}{\sqrt{r^2 - z^2}} = \frac{2r^3}{3}$$

we finally have:

$$\int_0^\infty G(z) z^3 dz = \frac{4}{3} \int_0^\infty p(r) r^2 dr$$

In a similar way the other moments of z and r can also be calculated.

3.2   Shapes

3.2.1   Eigenfunction and Gaussian coil

With respect to $\gamma(r)$ equation (2.8) is an Abel integral equation and its solution (see App. 2.2.3) is:

$$\gamma(r) = \frac{1}{\pi} \frac{1}{r} \frac{d}{dr} \int_r^{+\infty} dz \frac{G(z) z}{\sqrt{z^2 - r^2}} \tag{3.8}$$

This permits us to recalculate measured $G(z)$ into $\gamma(r)$, but this approach to the treatment of experimental data is not very useful since this transformation includes divergent integral and differentiation. It is more convenient to fit experimental data by an analytically known $G(z)$. For most conventional isotropic particles an analytical representation of $G(z)$ is discussed below.

Forward (2.8) and backward (3.8) transformations involve the same projection integral operator $\hat{x}$:

$$\begin{cases} G = \hat{x}\gamma \\ \gamma = \frac{1}{\pi}\frac{1}{r}\frac{d}{dr}\hat{x}G \end{cases} \tag{3.9}$$

The eigenfunction of integral operator $\hat{x}$ should also be an eigenfunction of differential operator:

$$\frac{1}{r}\frac{d}{dr}$$

The eigenfunction is Gaussian:

$$G(z) = e^{-\frac{z^2}{6\langle R_g^2 \rangle}}$$

This correlation function corresponds to the unperturbed Gaussian coil model for polymers.

3.2.2   Sphere

For uniform homogeneous spherical particles the conventional correlation function is known analytically [8]:

$$\gamma_p(r) = \rho^2 v \gamma(r) \tag{3.10}$$

where:

$$\gamma(r) = 1 - \frac{3}{4}r + \frac{1}{16}r^3 \tag{3.11}$$

where r is a reduced radius of a sphere,

Substituting (3.11) into (2.8) we get SESANS auto correlation function for a homogeneous sphere:
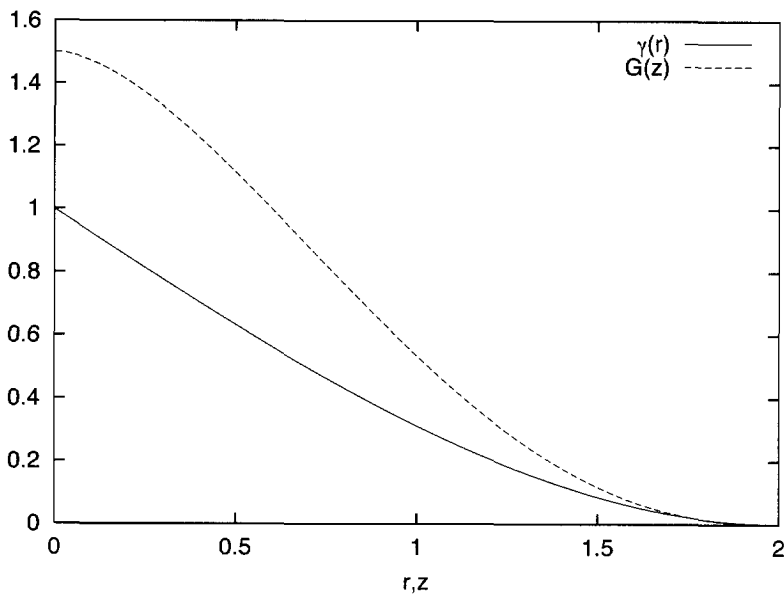
Figure 3.2: Conventional auto correlation function (solid line) and SESANS auto correlation function (dotted line) for a homogeneous sphere.

$$G(z) = \sqrt{1 - \left(\frac{z}{2}\right)^2} \left(1 + \frac{1}{8}z^2\right) + \frac{1}{2}z^2 \left(1 - \left(\frac{z}{4}\right)^2\right) \ln \left(\frac{z}{2 + \sqrt{4 - z^2}}\right)$$

(3.12)

and the total cumulative scattering probability is:

$$G_c(0) = \frac{N\rho^2 v_{\frac{3}{2}}^2 R\lambda^2}{S} = \frac{3}{2}\varphi\rho^2\lambda^2 tR$$

(3.13)

3.2.3   Hollow sphere

The hollow sphere is an important practical model describing a wide range of colloids. Let us consider a dimensionless case and characterize our hollow sphere by reduced parameters. The hollow sphere has an outer radius, $r_{out} = 1$, and inner radius, $r_{in} < 1$ (both reduced to the outer radius R). The reduced thickness is:

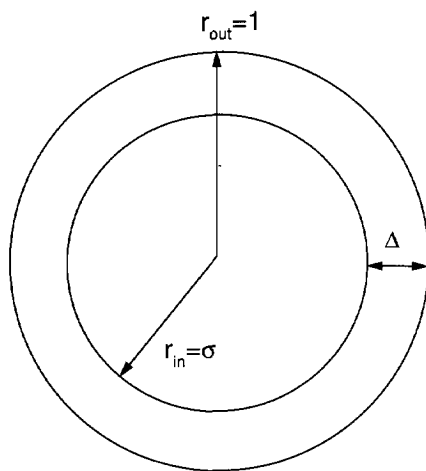$$\Delta = \frac{r_{out} - r_{in}}{r_{out}}$$

Figure 3.3: Hollow sphere

The reduced inner radius is:

$$\sigma = 1 - \Delta$$

$$r_{in} = \sigma r_{out}$$

The volume of a spherical layer is:

$$\Delta v = \frac{4}{3}\pi(r_{out}^3 - r_{in}^3) = \frac{4}{3}\pi r_{out}^3(1 - \sigma^3) = v(1 - \sigma^3)$$

where $V = \frac{4}{3}\pi r_{out}^3$ is the volume of the whole particle.

Calculations of $G(z)$ for such a hollow sphere can be found in Appendix 3.2.4

$G(z)$ for a hollow sphere has two distinct regions. We have two characteristic sizes. At distances $2 \geq r \geq 2 - \Delta$ hollow sphere behavior is indistinguishable from those of solid sphere (see Figs.3.5 and 3.6 in Appendix 3.2.4). All autocorrelations of course are limited by 2 radii. For $\Delta \geq r \geq 0$ we have initial decay due to disappearance of "Δ-layer" correlation.
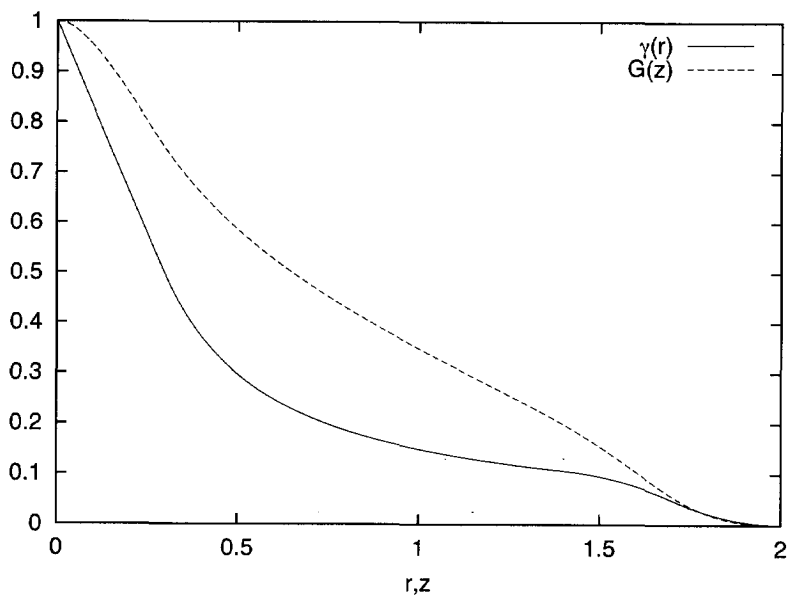
Figure 3.4: Conventional auto correlation function (solid line) and SESANS auto correlation function (dotted line) for a hollow sphere with $\Delta = 0.3$

3.2.4 Hollow sphere auto correlation function

The conventional auto correlation function of a hollow sphere is known analytically (Glatter,1979):

$$\gamma(r) = \rho^2 v \times$$

$$\begin{cases} 1 - \frac{3}{4}r + \frac{1}{16}r^3 & 2 \geq \chi \geq 2 - \Delta \\ \frac{3}{8}\frac{(1-\sigma^2)^2}{r} - \sigma^3 + \frac{3}{4}\sigma^2 r - \frac{1}{16}r^3 & 2 - \Delta \geq r \geq 2 - 2\Delta \\ \frac{3}{8}\frac{(1-\sigma^2)^2}{r} & 2 - 2\Delta \geq r \geq \Delta \\ (1 - \sigma^3) - \frac{3}{4}(1 + \sigma^2)\chi + \frac{1}{8}r^3 & \Delta \geq r \geq 0 \end{cases}$$

or in a short notation:

$$\gamma(r) = \rho^2 v \times$$

$$\begin{cases} \gamma_0(r) & 2 \geq \chi r 2 - \Delta \\ \gamma_1(r) - \sigma^3 \gamma_0(\frac{r}{\sigma}) & 2 - \Delta \geq r \geq 2 - 2\Delta \\ \gamma_1(r) & 2 - 2\Delta \geq r \geq \Delta \\ \gamma_0(r) + \sigma^3 \left[\gamma_0(\frac{r}{\sigma}) - 2\right] & \Delta \geq r \geq 0 \end{cases}$$

where $\gamma_0(r)$ is a correlation function of a homogeneous sphere (see equation (3.10)) and

$$\gamma_1(r) = \frac{3}{8}\frac{(1 - \sigma^2)^2}{r}$$

$$G(z) = 2 \int_z^2 dr \frac{\gamma(r)r}{\sqrt{r^2 - z^2}}$$

Since in four different r regions $\gamma(r)$ is defined by different analytical expressions, we decompose integration in four corresponding regions. Further procedure is trivial. As a result of four different regions we have "layer projections" for $b \geq r \geq a$:

$$G(z, a, b) = 2 \int_a^b dr \frac{\gamma(r)r}{\sqrt{r^2 - z^2}}$$

Or in short notation used below:

$$G(z, a, b) = \int_a^b \gamma$$

This operation is schematically depicted in Fig 3.6.

After integration we have the following set of functions:

$$\begin{cases} 2 \geq z \geq 2 - \Delta \\ G(z) = G(z, z, 2) \end{cases}$$

$$\begin{cases} 2 - \Delta \geq z \geq 2 - 2\Delta \\ G(z) = \int_z^2 \gamma = \\ = \int_{2-\Delta}^2 \gamma + \int_{2-2\Delta}^{2-\Delta} \gamma = \\ = \int_{2-\Delta}^2 \gamma_0 + \int_{2-2\Delta}^{2-\Delta} \left(\gamma_1(r) - \sigma^3 \gamma_0 \left(\frac{r}{\sigma} \right) \right) = \\ = G_0(z, 2 - \Delta, 2) + G_1(z, 2 - 2\Delta, 2 - \Delta) - G_\sigma(z, 2 - 2\Delta, 2 - \Delta) \end{cases}$$

$$\begin{cases} 2 - 2\Delta \geq r \geq \Delta \\ G(z) = \int_z^2 \gamma = \\ = \int_{2-\Delta}^2 \gamma + \int_{2-2\Delta}^{2-\Delta} \gamma + \int_\xi^{2-2\Delta} \gamma = \\ = \int_{2-\Delta}^2 \gamma_0 + \int_{2-2\Delta}^{2-\Delta} \left(\gamma_1(r) - \sigma^3 \gamma_0 \left(\frac{r}{\sigma} \right) \right) + \int_z^{2-2\Delta} \gamma_1(r) = \\ = G_0(z, 2 - \Delta, 2) + G_1(z, 2 - 2\Delta, 2 - \Delta) - G_\sigma(z, 2 - 2\Delta, 2 - \Delta) + G_1(z, z, 2 - 2\Delta) = \\ = G_0(z, 2 - \Delta, 2) - G_\sigma(z, 2 - 2\Delta, 2 - \Delta) + G_1(z, z, 2 - \Delta) \end{cases}$$

$$\begin{cases} \Delta \geq z \geq 0 \\ G(z) = \int_z^2 \gamma = \int_\Delta^2 \gamma + \int_z^\Delta \gamma = \int_\Delta^2 \gamma + \int_z^\Delta \gamma = \\ = \int_\Delta^2 \gamma + \int_z^\Delta \left[\gamma_0(r) + \sigma^3 \left[\gamma_0(\frac{r}{\sigma}) - 2 \right] \right] = \\ = G_0(z, 2 - \Delta, 2) - G_\sigma(z, 2 - 2\Delta, 2 - \Delta) + G_1(z, \Delta, 2 - \Delta) + G_0(z, z, \Delta) + \\ + G_\sigma(z, z, \Delta) - 2\sigma^3 \sqrt{\Delta^2 - z^2} \end{cases}$$

where

$$_a^b G_0(z) = 2 \int_a^b dr \frac{\gamma_0(r) r}{\sqrt{r^2 - z^2}} = 2 \left(\Gamma(b, z) - \Gamma(a, z) \right)$$

where

$$\Gamma(a, z) = \frac{1}{16} \sqrt{a^2 - z^2} \left[16 + \frac{a^3}{4} + \frac{3}{8} a(z^2 - 16) \right] + \\ \frac{3}{128} z^2 (z^2 - 16) \ln(a + \sqrt{a^2 - z^2})$$

$$_a^b G_\sigma(z) = \sigma^4 {}_{\frac{a}{\sigma}}^{\frac{b}{\sigma}} G(\frac{z}{\sigma})$$

$$G_1(\xi, a, b) = 2R \int_a^b dr \frac{\gamma_1(r)r}{\sqrt{r^2 - z^2}} = \tag{3.14}$$

$$= 2\frac{3}{8}(1 - \sigma^2)^2 \ln\left[\frac{b + \sqrt{b^2 - z^2}}{a + \sqrt{a^2 - z^2}}\right]$$

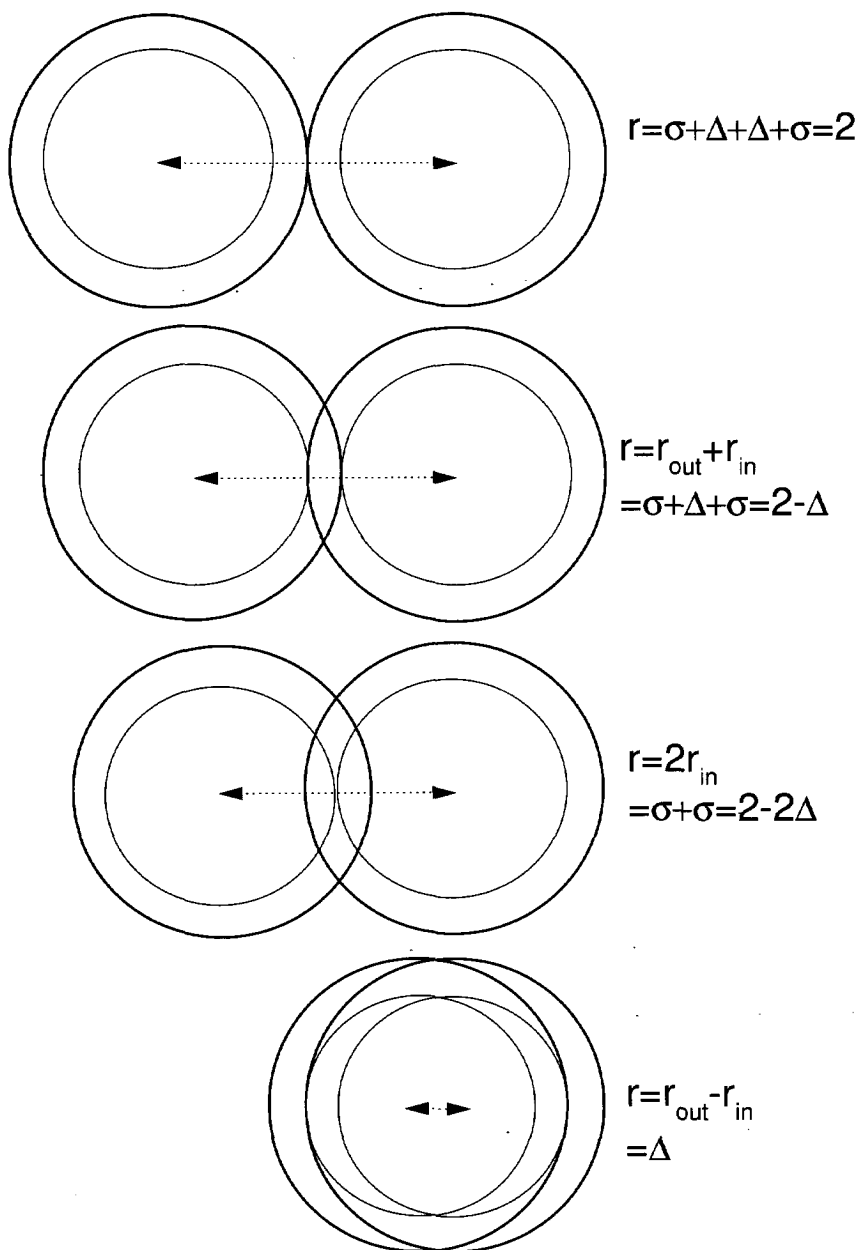These explicit functions can be directly used for fitting experimental data.

Figure 3.5: Geometrical interpretation of conventional auto correlation function $\gamma(r)$ for a hollow sphere.
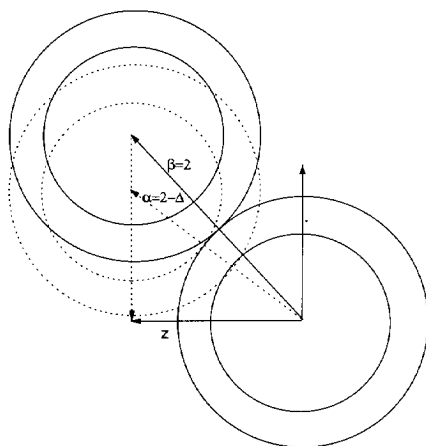
Figure 3.6: Projection of autocorrelation function of hollow sphere, where r runs from β to α covering the region where a hollow sphere and its ghost interfere as solid spheres.

Chapter 4

Correlation function of the excluded volume

This chapter introduces a correlation function of the excluded volume necessary for a real-space description of scattering from dense systems of spherical particles.

4.1 Correlation function of the excluded volume

We consider a system of homogeneous spherical particles. Let the total number of particles N occupy the volume V. The center of i-th sphere is located at a position $\mathbf{r}_i$ and is described by a scattering density $\rho(\mathbf{r} - \mathbf{r}_i)$:

$$\rho(\mathbf{r}_i) = \begin{cases} \rho & \text{if } |r| \leq 1 \\ 0 & \text{otherwise} \end{cases} \tag{4.1}$$

where ρ is a scattering length density of a homogeneous sphere. Spatial variables r and further a are in units of a sphere radius. The system of N particles is described by the contrast

$$\Delta\rho(\mathbf{r}) = \sum_{i=1}^{N} \rho(\mathbf{r} - \mathbf{r}_i) - \langle\rho\rangle \tag{4.2}$$

where

$$\langle\rho\rangle = \frac{1}{V}\int_V d^3\mathbf{r}\rho(\mathbf{r})$$

A spatial correlation function is defined as:

$$\gamma_N(\mathbf{r}) = \int_V \Delta\rho(\mathbf{r}')\Delta\rho(\mathbf{r}' - \mathbf{r})d^3\mathbf{r}' \tag{4.3}$$

If we substitute (4.2) to (4.3) we get:

$$\gamma_N(\mathbf{r}) = \int_V \sum_{i=1}^{N} [\rho(\mathbf{r}' - \mathbf{r}_i) - \langle\rho\rangle] \sum_{j=1}^{N} [\rho(\mathbf{r}' - \mathbf{r}_j - \mathbf{r}) - \langle\rho\rangle] \ d^3\mathbf{r}' \tag{4.4}$$

The diagonal terms in the summation describe correlations within a single particle, while the off-diagonal terms describe correlations between the particles. Separating the two types of correlations, we get:

$$\gamma_N(\mathbf{r}) = \sum_{i=1}^{N} \int_V \rho(\mathbf{r}')\rho(\mathbf{r}' - \mathbf{r})d^3\mathbf{r}' +$$

$$\sum\sum_{i\neq j} \int_V \rho(\mathbf{r}' - \mathbf{r}_i)\rho(\mathbf{r}' - \mathbf{r}_j - \mathbf{r})d^3\mathbf{r}' - \langle\rho\rangle^2 V \tag{4.5}$$

The first term gives N times the auto correlation function of a single particle

$$\int_V \rho(\mathbf{r}')\rho(\mathbf{r}' - \mathbf{r})d^3\mathbf{r}' = N\rho^2 v\gamma_{auto}(\mathbf{r})$$

where $\gamma_{auto}(\mathbf{r})$ is normalized. The second term in (4.5) gives the cross correlation function between all particles depending on their relative coordinates $\mathbf{r}_i - \mathbf{r}_j = \mathbf{a}$.

After ensemble averaging (4.5) can be rewritten as:

$$\gamma_N(\mathbf{r}) = N\rho^2 v \left[\int_V \gamma_{auto}(\mathbf{r} - \mathbf{a})\left(\delta(\mathbf{a}) + n(\mathbf{a}) - n\right)d^3\mathbf{a}\right] \tag{4.6}$$

where $n(\mathbf{a})$ is the number density of the particles. It can be expressed via the pair correlation function $g(\mathbf{a})$

$$n(\mathbf{a}) = ng(\mathbf{a})$$

where

$$n = \frac{N}{V} = \frac{\varphi}{v}$$

is the average number density of the particles, v is the volume of one particle and φ is the volume fraction of the particles.

Here we introduce the normalized "per particle" correlation function

$$\gamma(r) = \frac{\gamma_N(r)}{N\rho^2 v} \tag{4.7}$$

In normalized form (4.6) can be rewritten as

$$\gamma(\mathbf{r}) = \int_V \gamma_{auto}(\mathbf{r} - \mathbf{a}) \left(\delta(\mathbf{a}) + n(\mathbf{a}) - n\right) d^3\mathbf{a} \tag{4.8}$$

If the system is isotropic then (4.8) can be rewritten in a spherically symmetric form:

$$\gamma(r) = \gamma_{auto}(r) + \varphi \int_0^\infty \gamma_{cross}(r, a) \left[g(a) - 1\right] 3a^2 da \tag{4.9}$$

Equations (4.8) (Cartesian coordinates) and (4.9) (spherical coordinates) are real space equivalents of the classical Zernike and Prins equation [36]. The integration in (4.9) can be can be decomposed in two regions, $0 \le a < 2$ and $2 \le a < \infty$ (see fig.4.1):

$$\gamma(r) = \gamma_{auto}(r) - \varphi \int_0^2 \gamma_{ovl}(r, a) 3a^2 da +$$
$$\varphi \int_2^\infty \gamma_{cross}(r, a) \left[g(a) - 1\right] 3a^2 da \tag{4.10}$$

where $\gamma_{cross}(r, a)$ is a spherically averaged cross correlation function of a dumbbell [7]. The region $0 \le a < 2$ corresponds to the overlapping spheres. A correlation function for such structure was unknown until now. The derivation and the analytical form of correlation function of overlapping spheres $\gamma_{ovl}(r, a)$ can be found in the app.4.3.1 It is represented in fig.4.6. Appearance of the nonexisting structure of overlapping spheresis the consequence of the subtraction of the average density in (4.2). Upon subtraction of the average density, the probability to find a sphere inside the excluded volume formally charges from zero to -1. Therefore we have to count all overlapping spheres for $0 < a < 2$ and subtract them from the total correlation function The correlation function of overlapping spheres is integrated over the excluded volume yielding the correlation function of excluded volume (second term in (4.10)):

$$\gamma_{excl}(r) = \int_0^2 \gamma_{ovl}(r, a) 3a^2 da \qquad (4.11)$$

In analytical form it is presented in the app.4.3.2 and it is plotted in fig.4.2. This function is nonzero at $0 < r < 4$. Apparently spheres within the excluded volume affect correlations covering the maximum size of two overlapping spheres, which is the same as the minimum size of two touching spheres: $4R$. The last term in (4.10) is defined as structural correlation function:

$$\gamma_{struct}(r) = \int_2^\infty \gamma_{cross}(r, a) \left[g(a) - 1\right] 3a^2 da \qquad (4.12)$$

This correlation function depends on mutual arrangement of the particles and depends implicitly (via $g(a)$) on their density.

Combining (4.11) and (4.12) in (4.10) one gets:

$$\gamma(r) = \gamma_{auto}(r) - \varphi\gamma_{excl}(r) + \varphi\gamma_{struct}(r) \qquad (4.13)$$

The first term is independent on structure. The second term is a first approximation of structure and is proportional to the density. The structural correlation function can be calculated for a given pair correlation function using (4.12). A set of these functions for a hard-sphere liquid is presented on fig. 4.2.

4.2 Conclusion

Introduction of the correlation function of overlapping spheres and consequently, correlation function of the excluded volume allowed to complete a real-space description of scattering from dense systems. Both functions are calculated analytically for spherical particles. The excluded volume correlations are separated from the rest of the structure. The correlation function of the excluded volume gives the first approximation of structure, which is proportional to the particles' concentration.

4.3 Appendices

4.3.1 Correlation function of overlapping spheres

The auto correlation function of a sphere is given by:

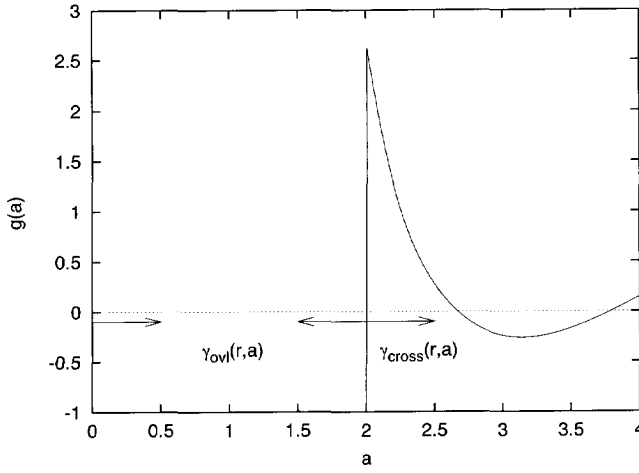$$\gamma_{auto}(r) = 1 - \frac{3}{4}r + \frac{1}{16}r^3 \qquad (4.14)$$

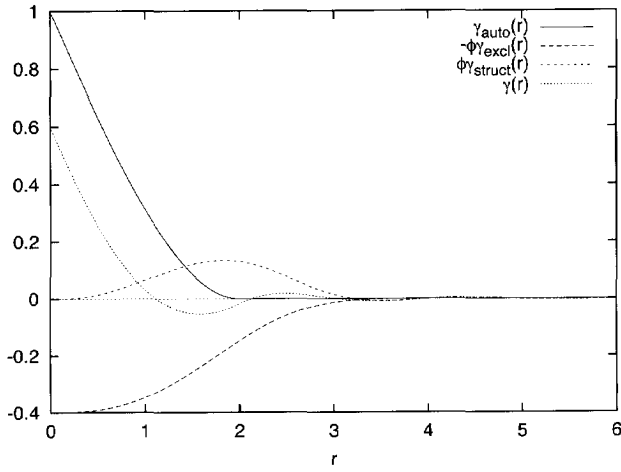Figure 4.1: Origin of the correlation function of overlapping spheres

Figure 4.2: Correlation functions by (9.1) for a hard-sphere liquid at a volume fraction $\varphi = 0.4$. Percus-Yevick pair correlation function was used for $g(a)$ in (4.12).

where ρ is a scattering density of a sphere and $v = \frac{4\pi}{3}$ is its volume (assuming the radius $R = 1$). The normalized correlation function is defined as a convolution

$$\gamma_{auto}(r) = \frac{1}{\rho^2 v} \int_0^\infty \rho(r - r')\rho(r')d^3\mathbf{r}' \qquad (4.15)$$

In general for homogeneous particles c.f is proportional to the intersection [1] volume of particle $\rho(r')$ and its host, shifted by a distance r.

For futher consideration we put $\rho = 1$.

A cross correlation function of a system of two particles equals to the intersection volume of a second particle with the ghost of the first one (see fig. 4.3).

If a ghost is shifted to the vector $\mathbf{r}$ with respect to its native sphere (first sphere), it appears to be shifted to the vector $\mathbf{r}' = \mathbf{r} - \mathbf{a}$ with respect to the second real sphere, shifted to the vector $\mathbf{a}$ with respect to the first real sphere. The intersection volume of first-ghost and second-real sphere is then given by:

$$\gamma_{cross}(r) = \gamma_{auto}(r')$$

The above intersection is realized at a single triplet of vectors $\mathbf{r}$, $\mathbf{r}'$ and $\mathbf{a}$, having a specific orientation in space. The distance between the second sphere and the ghost image of the shifted first one (see fig 4.3):

$$r'^2 = r^2 + a^2 - 2ar\cos\theta$$

If r' and θ are fixed we can rotate $\mathbf{r}'$ around $\mathbf{a}$ axis to count all possible directional realizations of r' to make the function isotropic:

$$\gamma_{cross}(r) = \int_{\cos\theta_{max}}^1 \gamma_{auto}(r')d(\cos\theta) = \qquad (4.16)$$

$$\int_{\cos\theta_{max}}^1 \gamma_{auto}\left(\sqrt{r^2 + a^2 - 2ar\cos\theta}\right)d(\cos\theta)$$

where $\xi_{min} = cos(\theta_{max})$ determines the widest angle at which spheres still intersect.

At an arbitrary θ_{max} three terms of (4.14) evaluate to the following expressions:

$$\int_{\xi_{min}}^1 d(\xi) = 1 - cos(\theta_{min}) = 1 - \xi_{min}$$

---

[1] The term *overlap* is used for two real spheres. Here the term *intersect* applied to the ghost-real sphere combination to avoid confusion with *overlap* meant for real-real combination.

$$-\frac{3}{4}\int_{\xi_{min}}^{1}\sqrt{r^2+a^2-2ar\xi}d\xi =$$

$$\frac{1}{4ar}\left(|r-a|^3 - \sqrt{r^2+a^2-2ar\xi_{min}}^3\right)$$

$$\frac{1}{16}\int_{\xi_{min}}^{1}\sqrt{r^2+a^2-2ar\xi}^3 d\xi =$$

$$\frac{1}{80ar}\left(|r-a|^5 - \sqrt{r^2+a^2-2ar\xi_{min}}^5\right)$$

$$\gamma_{ovl}(r,a) = 1 - \xi_{min}$$
$$+\frac{1}{4ar}\left(|r-a|^3 - \sqrt{r^2+a^2-2ar\xi_{min}}^3\right)$$
$$-\frac{1}{80ar}\left(|r-a|^5 - \sqrt{r^2+a^2-2ar\xi_{min}}^5\right) \tag{4.17}$$

For the interpenetrating spheres there are two regimes of intersection. If $r < 2-a$ spheres intersect at any $\cos\theta$ (see fig 4.4). For that regime $\xi_{min} = -1$ and (4.17) reduces to

$$\gamma_{ovl}(r,a) = 2 + \frac{1}{4ar}\left(|r-a|^3 - |r+a|^3\right)$$
$$-\frac{1}{80ar}\left(|r-a|^5 - |r+a|^5\right) \tag{4.18}$$

If $2-a < r < a+2$ then $\theta < \pi$ the touching condition is given by (see fig.4.5):

$$4 = a^2 + r^2 - 2ar\xi_{min}$$

$$\xi_{min} = \frac{a^2+r^2-4}{2ar} \tag{4.19}$$

and after substitution to (4.17) yields the same functional form as the cross correlation function (calculated earlier in [7]):

$$\gamma_{ovl}(r,a) = 1 - \frac{a^2+r^2-4}{2ar} + \frac{1}{4ar}\left(|r-a|^3 - 2^3\right)$$
$$-\frac{1}{80ar}\left(|r-a|^5 - 2^5\right) \tag{4.20}$$

If $a \to 0$ then (4.18) covers the whole region $0 < r < 2$ reduces to the well known auto correlation function of a sphere (4.14).

If $a \geq 2$ then (4.18) disappears and (4.20) is now a cross correlation function
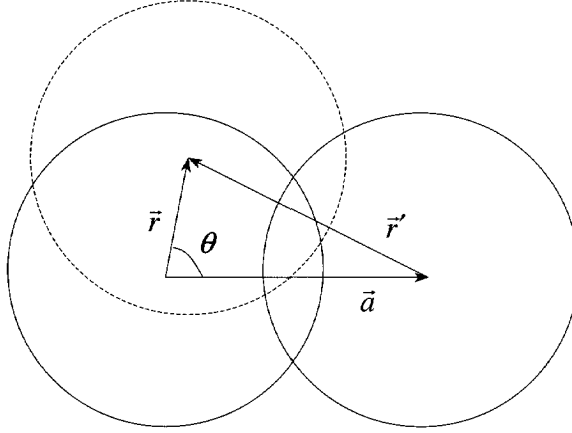
Figure 4.3: The correlation function of two overlapping spheres. The cross correlation function of such system is proportional to the overlapping volume of the left-ghost with right real sphere. The left-ghost particle being shifted by the distance $\mathbf{r}$ from its real counterpart stays at a distance $\mathbf{r}' = \mathbf{r} + \mathbf{a}$ so the overlap volume is given by $\gamma_{auto}(\mathbf{r}')$

$$r = 2(1-a)$$

$$\theta_{max} = \pi$$

$$\vec{r}$$
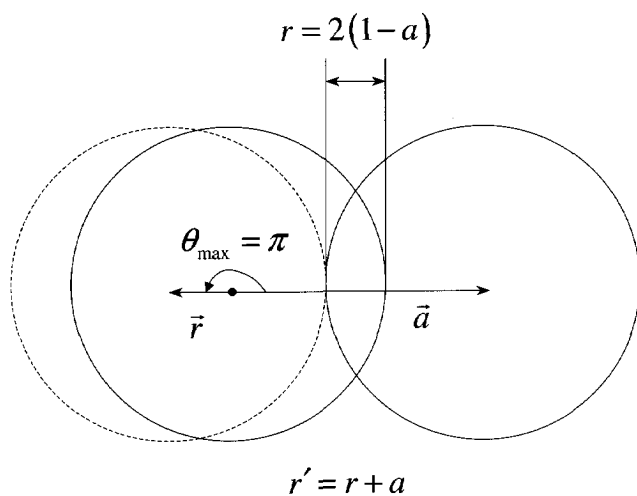
$$\vec{a}$$

$$r' = r + a$$

Figure 4.4: The geometry of unconditional overlap. If the left-ghost is shifted to the distance $r \leq 2 - a$ it intersects with the right real sphere at any θ, which makes the lower limit of integration in (4.17) $\cos(\theta_{max}) = -1$.
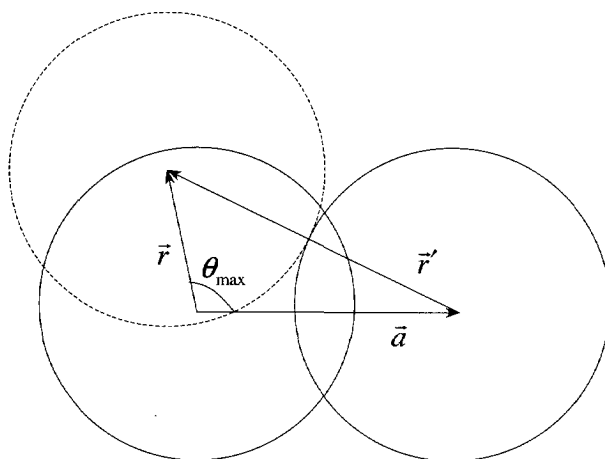
Figure 4.5: The touching condition by (4.19) defines the maximum angle θ at which the left ghost and the right real spheres still intersect.
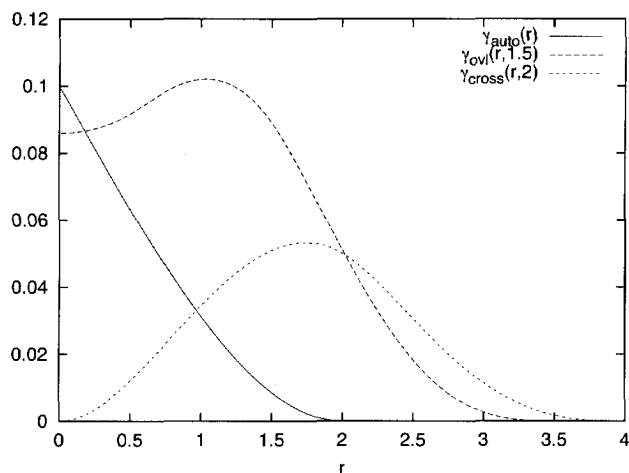
Figure 4.6: Correlation functions for spherical particles: solid line - auto correlation function (reduced by factor 10) by (4.14), dashed line - correlation function of overlapping spheres by (4.18) (a=1.5), dotted line is a cross correlation function by (4.20) with a=2.

4.3.2 Correlation function of the excluded volume

$$\gamma_{excl}(r) = \int_0^2 \gamma_{ovl}(r, a) 3a^2 da \qquad (4.21)$$

$$\gamma_{excl}(r) = \qquad (4.22)$$

$$1 - \frac{3}{16}r^3 + \frac{9}{160}r^4 - \frac{r^6}{2240} \quad \text{if } 0 \le r \le 2$$

$$8 - \frac{144}{35r} - \frac{18r}{5} + \frac{5r^3}{16} - \frac{9r^4}{160} + \frac{r^6}{2240} \quad \text{if } 2 \le r \le 4$$

Chapter 5

Interacting particles

This chapter presents (Spin-Echo) SANS correlation functions describing small-angle scattering on dense systems of spherical particles. (Spin-Echo) small-angle correlation functions and associated correlation lengths for a single sphere, a dumbbell, excluded volume and structure are introduced. It is shown that the correlation length is proportional to the cumulative scattering probability. This approach is applied to a hard-sphere liquid.

5.1   SESANS correlation functions

Let us consider a system of N homogeneous spheres with scattering density ρ and radius R occupying the volume V. The conventional correlation function of such system is known [7, 17]. If we substitute a normalized conventional correlation function in (2.8) and express spacial coordinates in terms of sphere's radius we get:

$$G_c(z) = 2\varphi(\Delta\rho)^2\lambda^2 tR \int_z^{+\infty} dr \frac{\gamma(r)r}{\sqrt{r^2 - z^2}} \qquad (5.1)$$

Here we introduce a reduced correlation function

$$G(z) = \frac{G_c(z)}{\varphi(\Delta\rho)^2\lambda^2 tR} \qquad (5.2)$$

so (5.1) can be rewritten in a simplier form:

$$G(z) = 2 \int_z^{+\infty} dr \frac{\gamma(r)r}{\sqrt{r^2 - z^2}} \tag{5.3}$$

The conventional correlation function can be presented as a set of three contributions [17]:

$$\gamma(r) = \gamma_{auto}(r) - \varphi\gamma_{excl}(r) + \varphi\gamma_{struct}(r) \tag{5.4}$$

where γ_{auto} is the auto correlation function of a single sphere, $\gamma_{excl}(r)$ is the correlation function of excluded volume and

$$\gamma_{struct}(r) = \int_2^{\infty} \gamma_{cross}(r, a) \left[g(a) - 1\right] 3a^2 da \tag{5.5}$$

is the structural correlation function

The same decomposition can be made for SESANS correlation function:

$$G(z) = G_{auto}(z) - \varphi G_{excl}(z) + \varphi G_{struct}(z) \tag{5.6}$$

where G_{auto}, G_{excl} and G_{struct} are projections if their respective conventional counterparts according to (5.3).

G_{auto} was calculated in [15], G_{excl} is given in app.5.5.2 and G_{struct} is

$$G_{struct}(r) = \int_2^{\infty} G_{cross}(z, a) \left[g(a) - 1\right] 3a^2 da \tag{5.7}$$

where $G_{cross}(z, a)$ given in app.5.5.1

5.2 Correlation length

A projection of a correlation function is a correlation length [6]:

$$G(0) = 2 \int_0^{\infty} \gamma(r) dr = \xi \tag{5.8}$$

According to (5.6) it can be decomposed into three contributions:

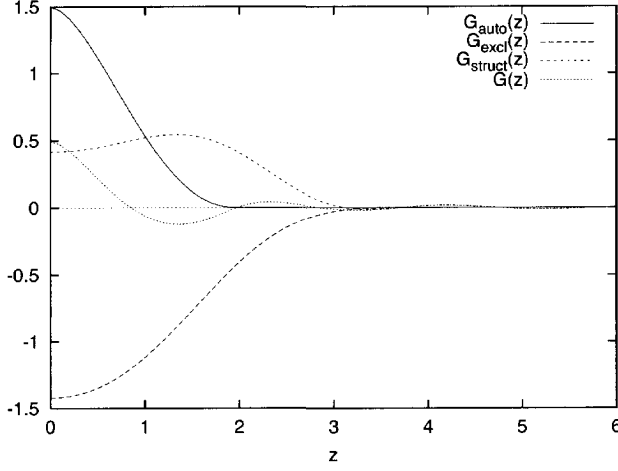$$\xi = \xi_{auto} - \varphi\xi_{excl} + \varphi\xi_{struct} \tag{5.9}$$

Figure 5.1: $G(z)$ for a hard-sphere liquid at volume fraction $\varphi = 0.4$. Percus-Yevick pair correlation function was used for $g(a)$. in (5.7).

where

$$\xi_{auto} = 2 \int_0^2 \gamma_{auto}(r)dr = \frac{3}{2} \tag{5.10}$$

is a correlation length of a single sphere (in terms of its radius).

$$\xi_{excl} = 2 \int_0^4 \gamma_{excl}(r)dr = \frac{36}{35}\left(9 - 8\ln(2)\right) \approx 3.55 \tag{5.11}$$

is a correlation length of the excluded volume contributes with the minus sign to the total correlation length. Both ξ_{auto} and ξ_{excl} do not depend on the mutual arrangment of spheres.

The last term is a structural correlation length

$$\xi_{struct} = 2 \int_2^\infty \left(g(a) - 1\right)\xi_{cross}(a)3a^2 da \tag{5.12}$$

where we define a cross correlation length of 2 spheres (forming a dumbbell with a distance a between centers of the spheres):

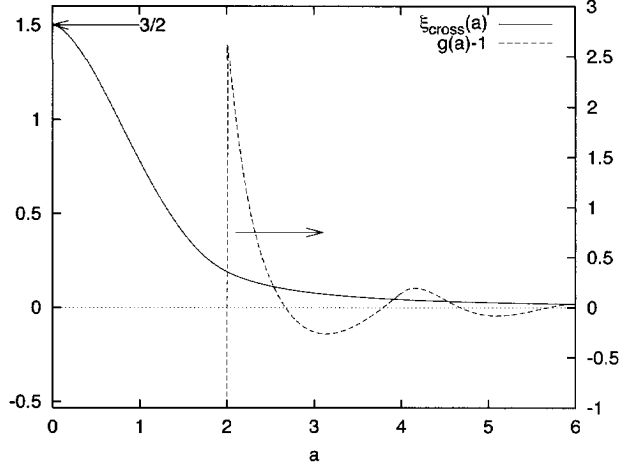$$\xi_{cross}(a) = 2 \int_{a-2}^{a+2} \gamma_{cross}(r,a)dr \tag{5.13}$$

Figure 5.2: $\xi_{cross}(a)$ and $g(a) - 1$ to be integrated according to (5.12).

The calculations and the analytical expression for ξ_{cross} is given in the app.5.5.3 As an example consider a dumbbell of touching spheres. Additionally to $\xi_{auto} = \frac{3}{2}$ we have

$$\xi_{cross}(2) = \frac{13}{10} - \frac{8}{5}\ln 2 \approx 0.19 \qquad (5.14)$$

which is due to a correlation of neutrons scattered on different spheres of a dumbbell. In total we have for a dumbbell $\xi_{dumbbell} = 1.50 + 0.19 = 1.69$. If we have an ensemble of particles we apply (5.12), which physically is a summation of correlation lengths of all dumbbells formed by a central sphere with neighbours weighted with probability $g(a)$. A general expression for the correlation length of the system of spheres can be written as:

$$\xi = \frac{3}{2} - \frac{36}{35}\left(9 - 8\ln 2\right)\varphi + \varphi\xi_{struct} \qquad (5.15)$$

Taking into account (5.1) the total cumulative scattering probability is proportional to the correlation length:

$$G_c(0) = \varphi(\Delta\rho)^2\lambda^2 tR\xi \qquad (5.16)$$

5.3 Hard sphere liquid

Here we use a hard sphere liquid as an example of application of three correlation lengths described in previous section. Since $g(a)$ for a hard-sphere liquid is determined only by φ, the correlation length as well as the total scattering probability is a function of only one variable φ. Fig.5.3 shows how three correlation lengths depend on φ. Due to the increasing number of neighbours the structural correlation length increases with increasing φ. At the same time the correlation length of the excluded volume linearly increases (with negative sign) due to the increase of the number of particles unable to penetrate the excluded volume. In this "per particle" representation the auto correlation length is a zeroth order approximation, the correlation length of the excluded volume is a first order approximation and the structural correlation is the rest. The corresponding dependencies for $G_c(0)$ and $\Delta P(0)$ are presented in fig.5.4. The parameters are taken for actually measured sample [16]. The total cumulative scattering probability of a hard-sphere liquid has a maximum at $\varphi \approx 0.33$ (see fig. 5.4). The position of this maximum is a property of a hard-sphere system. The full correlation functions and SESANS signal for any given φ can be calculated using the tools described in the previous sections. (see fig.5.1).

5.4 Conclusions

SESANS is a particular implementation of a generic real-space small-angle scattering device measuring correlations in one direction. Unlike reciprocal-space scattering techniques it is free from the multiple scattering problem. The total correlation function of a system of spherical particles is a sum of the correlation function of a single sphere, correlation function of the excluded volume and the structural correlation function The correlation function of the excluded volume is a first structural approximation. The same decomposition holds for correlation length, which is a measure of intensity of scattering on respective structural features. The total depolarization level in SESANS equals true scattering probability. The logarithm of the saturation level of polarization equals total cumulative scattering probability, which is proportional to the correlation length. For a hard-sphere liquid the maximum of the total cumulative scattering probability was found at the volume fraction $\varphi \approx 0.33$. The paper presents a complete description of small-angle scattering on a system of spherical particles in real space.
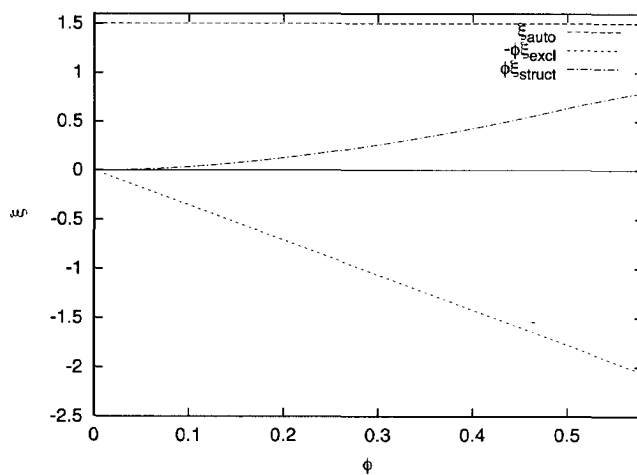
Figure 5.3: Correlation lengths for a hard-sphere liquid depending on volume fraction φ: solid line - correlation length of a sphere, dashed line - correlation length of the ecluded volume, dotted line - structural correlation length. The Percus-Yevick pair correlation function was used to calculate ξ_{struct}.
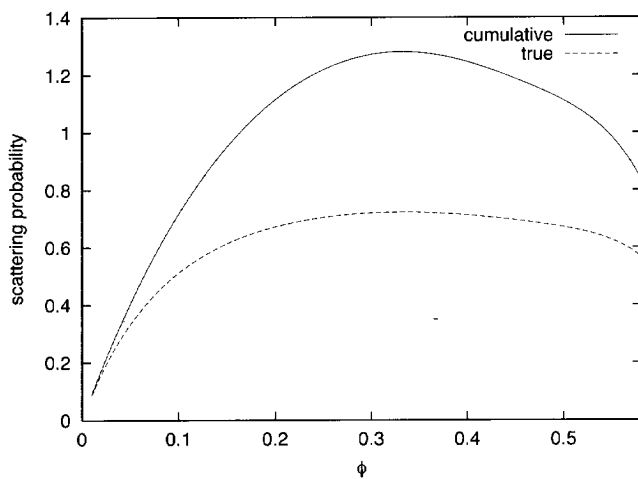
Figure 5.4: Scattering probabilities for a hard sphere liquid as functions of volume fraction. Solid line - total cumulative scattering probability $G_c(0)$, dashed line - total true scattering probability (or depolarization $\Delta P(0)$ in terms of SESANS).

5.5   Appendices

5.5.1   (SE)SANS cross correlation function for spherical particles

$$G(z,a) =$$
$$\begin{cases} G_l(a-2,a,z) & +G_r(a,a+2,z) & \text{if } z < a-2 \\ G_l(z,a,z) & +G_r(a,a+2,z) & \text{if } a-2 < z < a \\ & G_l(z,a+2,z) & \text{if } a < z < a+2 \\ & 0 & \text{if } a+2 < z \end{cases}$$

where

$$G_l(b,c,z) = \frac{1}{9600a} \left(\alpha_l(b) - \alpha_l(c) + \beta_l(b,c) \right)$$

$$G_r(b,c,z) = \frac{1}{9600a} \left(\alpha_r(b) - \alpha_r(c) + \beta_r(b,c) \right)$$

$$\alpha_l(\xi) = \sqrt{\xi^2 - z^2} \left(f_1(a) + f_2(a,\xi) + f_3(a,\xi,z) \right)$$

$$\alpha_r(\xi) = \sqrt{\xi^2 - z^2} \left(f_1(-a) - f_2(-a,\xi) + f_3(a,\xi,z) \right)$$

$$\beta_l(b,c) =$$
$$15(f_4(a) + f_5(a) + 15az^4) \ln\left(\frac{b + \sqrt{b^2 - z^2}}{c + \sqrt{c^2 - z^2}} \right)$$

$$\beta_r(b,c) =$$
$$-15(f_4(-a) - f_5(-a) + 15az^4) \ln\left(\frac{b + \sqrt{b^2 - z^2}}{c + \sqrt{c^2 - z^2}} \right)$$

$$f_1(a) = -600(4+a)a(-2+a)^2$$

$$f_2(a,\xi) = 600(4 - 6a + a^3)\xi$$

$$f_3(a,\xi,z) = -400(-2+a^2)\xi^2 + 150a\xi^3 - 24\xi^4$$
$$-(800(-2+a^2) - 225a\xi + 32\xi^2)z^2 - 64z^4$$

$$f_4(a) = 8(-2+a)^3(4 + (6+a)a)$$
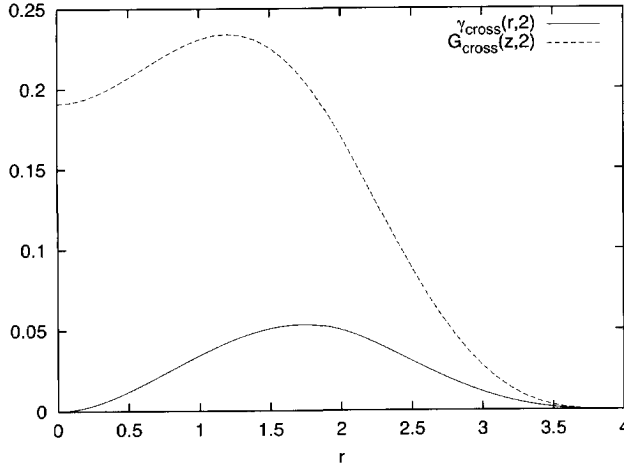
$$f_5(a) = 40(4 - 6a + a^3)z^2$$

Figure 5.5: Conventional and SESANS cross correlation functions for spherical particles.

5.5.2 (SE)SANS correlation function of the excluded volume

$$G_{excl}(z) = \begin{cases} G_1(z) & \text{if } 0 \leq z \leq 2 \\ G_2(z) & \text{if } 2 \leq z \leq 4 \end{cases} \tag{5.17}$$

where

$$
\begin{aligned}
G_1(z) = \tfrac{1}{78400} \Big[& \\
-16\sqrt{4-z^2} \, & (39672 + 2523z^2 - 580z^4 + 4z^6) \\
+4\sqrt{16-z^2} \, & (124704 + 9735z^2 - 1112z^4 + 8z^6) \\
& +11025z^4 \ln z + \\
105 \big\{ (6144 + 2688z^2 - 280z^4) & \ln \left(2 + \sqrt{4-z^2} \right) \\
- (6144 + 2688z^2 - 175z^4) & \ln \left(4 + \sqrt{16-z^2} \right) \big\} \Big]
\end{aligned}
$$

and

$$
\begin{aligned}
G_2(z) = & \\
\frac{1}{78400} \Big[4\sqrt{16-z^2} \, & \left(124704 + 9735z^2 - 1112z^4 + 8z^6 \right) \\
-105 \left(-6144 - 2688z^2 + 175z^4 \right) & \ln \left(\frac{z}{4 + \sqrt{16-z^2}} \right) \Big]
\end{aligned}
$$

5.5.3 Cross correlation length of two spheres

$$\xi_{cross}(a) = \frac{1}{20}(a^2 + 22) \tag{5.18}$$

$$+\frac{1}{80a}(a-2)^3(a(a+6)+4)\ln|a-2|$$

$$-\frac{1}{40}a^2(a^2-20)\ln a$$

$$+\frac{1}{80a}(a+2)^3(a(a-6)+4)\ln(a+2)$$

Part II

Experiment

Chapter 6

Hard-sphere colloids

6.1   Correlation functions

Here we consider correlation functions describing the system of hard sphere particles, which we used to fit the experimental results.

The simplest case is that of isolated particles which experimentally corresponds to the colloid dilute enough to avoid interparticle interaction. In that case we need only the particle autocorrelation function $\gamma_{auto}(r)$. It has an analytical representation [9] and the corresponding SESANS correlation function $G_{auto}(z)$ as well [15]. The total depolarization level for a dilute solution of spherical particles is known [2]. The next case is when the concentration of particles is high enough for the appearance of pair correlations. In that case we have to take into account pair correlations, described by the cross correlation function $\gamma_{cross}(r)$

$$\gamma(r) = \gamma_{auto}(r) + \gamma_{struct}(r) \tag{6.1}$$

where the cross term is

$$\gamma_{struct}(r) = 4\pi n \int \gamma_{cross}(r, a)h(a)a^2 da \tag{6.2}$$

where $h(r) = g(r) - 1$, $g(r)$ being the pair correlation function and $n = \frac{N}{V}$ the particle number density (see, for instance, [11]). Functions $\gamma_{cross}(r, a)$ for spheres are known analytically [7]. The similarity between $G(z)$ and $g(r)$ is shown in Fig. 6.1.

The last case is a polycrystalline colloid. The structural correlation term can be represented as:

$$\gamma_{struct}(r) = \left\langle n \int_V \gamma_{cross}(\mathbf{r}')h(\mathbf{r} + \mathbf{r}')d\mathbf{r}' \right\rangle_\Omega \tag{6.3}$$

For the crystalline case the pair correlation function for a random hexagonal close packed structure was used. It can be represented as a set of delta functions:

$$h(\mathbf{r}) = \sum_i \delta(\mathbf{r} - \mathbf{r_i}) \tag{6.4}$$

where the index i runs over all lattice points.

After the cross term is rotationally averaged according to (6.3), the structural correlation function reads

$$\gamma(r) = \gamma_{auto}(R) + \sum_j M_j \gamma_{cross}(r, a_j) \tag{6.5}$$

The index j runs over shells located at a distance a_j from the central atom and containing M_j spheres. The SESANS counterpart of the cross term $G_{cross}(r, a)$ is known analytically.

The fitting curves for liquids represented in the figures below use Percus-Yevick solution with a Henderson-Grundke correction for the structure factor [30]. They are numerically calculated using the reciprocal space representation of $G(z)$ by Eq. 2.2. We could have used the real space representation by Eq. 6.2, but the software which was at our disposal calculated $g(r)$ up to 4 diameters only. In the crystalline case the real space representation by Eq. 6.5 was used directly. For all calculations we assumed monodisperse colloids in order to keep the calculations simple.
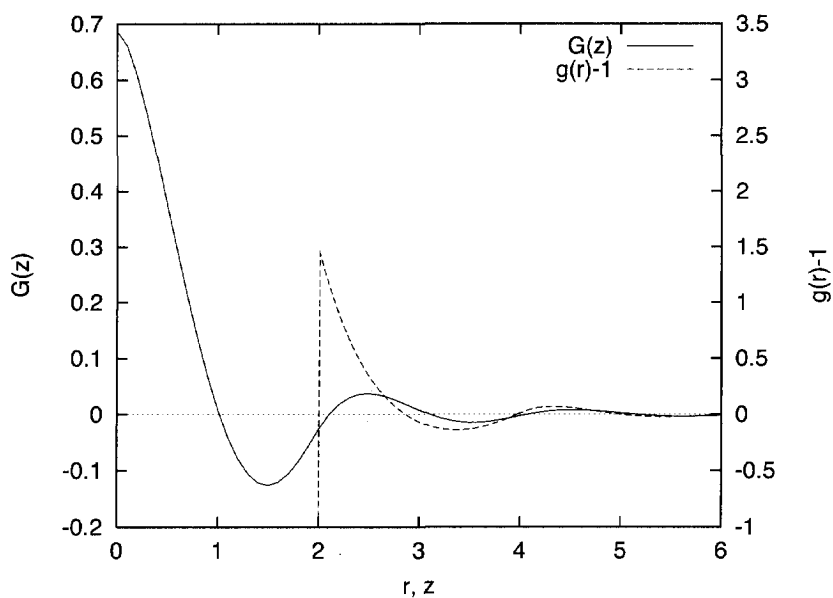
Figure 6.1: The SESANS correlation function $G(z)$ for a colloidal hard sphere liquid at volume fraction $\varphi = 0.3$ and the pair distribution function $g(r)$ for the same system. Variables z and r are normalized to the radius of a sphere.

6.2   Sample

As a source of particles we used sterically stabilized silica spheres suspended in cyclohexane. The density of the particle's material was determined to be 2.02 ± 0.10 g/cm^3 (DMA5000 densitymeter), which is somewhat smaller than that of bulk silica. The radius of the particles determined by the dynamic light scattering was 160 nm. TEM measurements yield the radius of the particles 153 nm and polydispersity 6.2 %. The particles were covered by a sterically stabilizing layer of Polyisobutene, 4-5 nm nanometers thick. The initial solution was dried under low (≈ 0.1 atm) pressure during 12 hours. Dry particles were then redispersed in deuterated cyclohexane. Directly after redispersion the sample appeared macroscopically homogeneous. A deuterated solvent was used in order to maximize the scattering contrast and minimize incoherent scattering. Three concentrations were prepared: 1 - dilute solution ($\phi_V = 0.055$) in a 10 mm thick cell, 2 - semidilute solution ($\phi_V = 0.27$) in a 5 mm thick cell, 3 - concentrated solution ($\phi_V = 0.32$) in a 1 mm thick cell. (Quoted volume fractions were known approximately during the preparation. Exact values were determined as a result of fitting.) All cells were 10 mm wide and 40 mm heigh. The thicknesses of samples were chosen such as to give considerable depolarisation, but not close to zero saturation level. The samples were illuminated by the neutron beam framed by a cadmium diaphragm 8.5 mm high and 7.5 mm wide which was mounted immediately in front of the cell.

6.3   Dilute solution

The dilute solution was prepared in order to observe non-interacting particles. On one hand we should use as low concentration as possible, but on the other hand we should keep the concentration high enough to keep the scattering probability high. The initially prepared homogeneous dilute solution completely settles during few days. Measurements were taken in a few steps of few hours each. Immediately before each measurement the sample was shaken to develop homogeneous structure. During the few hours of one measurement step the sample remained homogeneous.

For a dilute solution we can neglect pair correlations and the cross term drops out. The auto correlation term is nonzero only for distances less than the diameter of a sphere indicating that there is no correlation beyond the maximum size of a particle. As can be seen from fig.7.1, there is a saturation level reached at $z = 2R$. This constitutes the fact that there is no correlation

between particles and they can be considered non-interacting.

The fit determines two parameters independently: $R = 149$ nm and $(1 - \phi_V)\phi_V(\Delta\rho)^2$. The value of $R = 149$ nm is lower than those given by TEM (153 nm), which gives the lower bound of the radius due to shrinkage of the particles upon drying and DLS (160nm), which gives the upper bound of the radius due to hydrodynamic effects. The fact that SESANS value of the radius is less than that measured by TEM might be due to an error in determination of the z values. A systematic error in z value of a few percent can be due to the uncertainties in determination of the neutron wavelength λ ($\delta\lambda/\lambda$=0.01, which gives ± 3 nm uncertainty in z) and the foil inclination angle θ_0 ($\frac{\delta \cot\theta_0}{\cot\theta_0}$=0.04, which gives ± 6 nm uncertainty in z). In addition there is also an error due to the counting statistics. Including all mentioned errors the radius of the particle should be estimated as $R = 149 \pm 7$ nm. So within all the error bars, the SESANS technique is consistent with the two other methods.

In order to separate $(1 - \phi_V)\phi_V$ from $(\Delta\rho)^2$ a semidilute solution was used, which yields $\phi_V = 0.055$. For the ideal monodisperse hard sphere liquid for the actual value $\phi_V = 0.055$ the first minimum due to the excluded volume is already supposed to emerge, but in our case we do not see it due to the polydispersity.

6.4   Semidilute solution

In order to observe the appearance of pair correlations between particles a semidilute solution was used (see fig.6.4).

Unlike the dilute solution not only the saturation level $G(0)$, but also $G(z)$ depends on the volume fraction ϕ_V. The scattering contrast $\Delta\rho$ affects only the total level of depolarization $G(0)$, but not $G(z)$, which gives the possibility to determine ϕ_V and $\Delta\rho$ independently, which is not possible in case of the dilute solution. We fixed the value of the radius R obtained from the fit of the dilute solution and determined $\phi_V = 0.27$ and $\Delta\rho = 3.6 \cdot 10^{10} cm^{-2}$. The last value yields the scattering density of silica equal to $\rho_{silica} = 3.1 \cdot 10^{10} cm^{-2}$ which is consistent with the theoretically expected value $\rho_{silica} = 3.2 \cdot 10^{10} cm^{-2}$ (using the measured mass density of silica particles $2.02\frac{g}{cm^3}$). In principle, all three parameters R, ϕ_V and $\Delta\rho$ can be determined independently using the semidilute solution only.
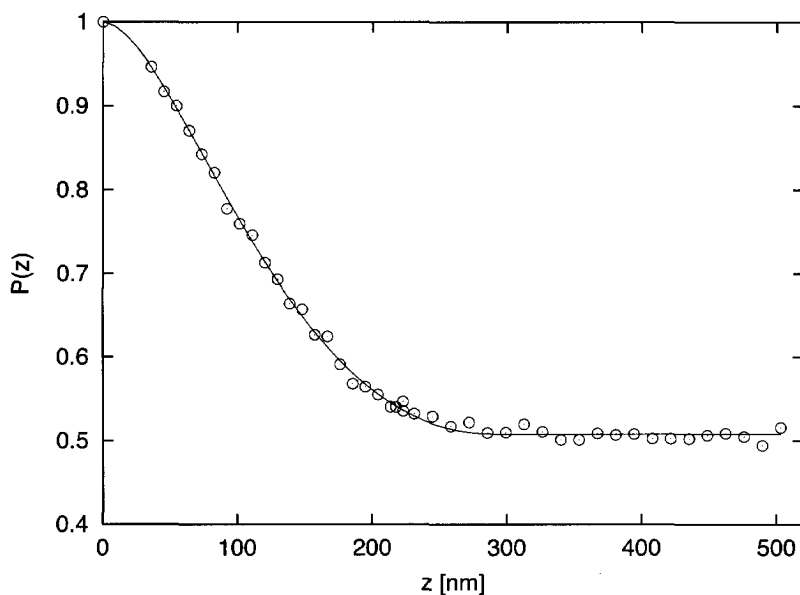
Figure 6.2: Dilute suspension of hard spheres. Error bars are approximately equal to the size of the circles. The same holds for the rest of the figures where error bars are absent. The solid line is the calculated curve for isolated spherical particles using $G_{auto}(z)$ by (3.12) with $\phi_V = 0.055$, $R = 149nm$.
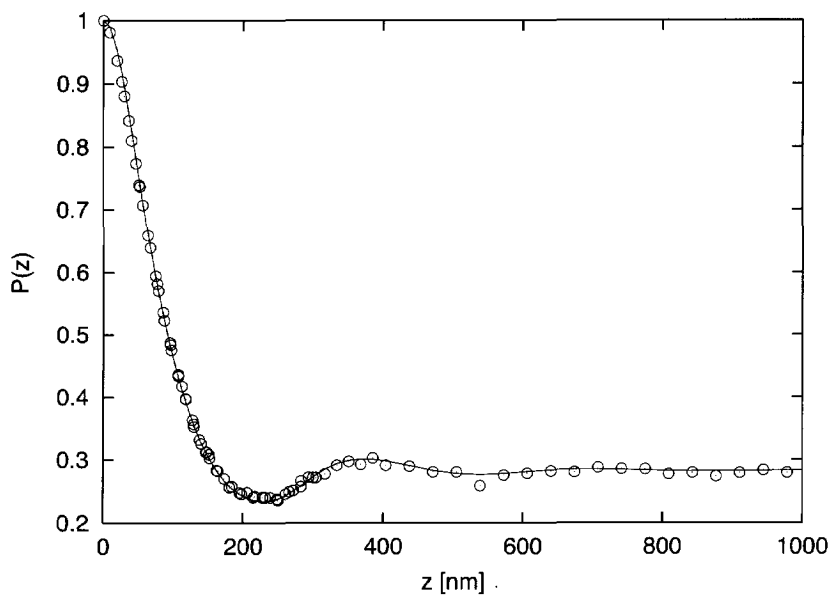
Figure 6.3: Semidilute suspension of hard spheres. The line is the calculation for the Percus-Yevick solution for a hard sphere liquid with $\phi_V = 0.27$ and $R = 149nm$.

6.5   Concentrated solution

A concentrated solution was prepared in order to observe the crystallisation process as a result of sedimentation induced by gravity. The volume fraction of silica in the initially prepared homogeneous solution was $\phi_V = 0.32$, which was determined by the fit in fig.6.5. The solution kept a visibly homogeneous structure for a few days. Measurements for the homogeneous solution presented in fig.6.5 were taken within several hours while the sample remained homogeneous. That assured uniformity of the volume fraction along the height of the sample during measurement. The fitting curve in fig.6.5 does not reach 1 at z=0 because we suspect that P_0 was not determined very precisely by measurement and we left P_0 as a fitting parameter.

Since the difference in mass density of the silica particles and the solvent was approximately 1.2 $\frac{g}{cm^3}$, the particles settled to the bottom of the cell. The gravitational length of the colloid $l_g = kT/\Delta\rho g V = 3$ cm. The gravitational length is the ratio of thermal energy to the gravitation (corrected for buoyancy) force and gives the length on which the work of gravitation (corrected for buoyancy) force is comparable to the thermal energy. The height of the sample exposed to the beam (0.85 cm) is of the same order of magnitude as the gravitational length which suggests a strong influence of gravitation on that length scale and causes sedimentation of the particles on the bottom of the cell. On the other hand l_g is much larger than the particle size so that the gravity is not expected to affect the local structure. The suspension after 1 week of rest showed a macroscopic phase separation into 3 parts with clear boundaries. The top part was transparent solvent, the middle and the bottom contained colloidal particles. The middle part was more opaque than the bottom part. During the first two weeks after preparation the bottom part grew at the expense of the middle part. Both parts were then measured after two weeks. Results are presented in Fig. 6.5.

It can be seen from the figure that the saturation level of the middle part is 0.79 and that of the bottom part is 0.84. That is an indication that the average concentration of those parts of the sample differs by a few percents. Apparently the sample has gradually increasing concentration of the particles from the top to the bottom and the measured SESANS signal covers a distribution of volume fractions within the vertical size of the diaphragm. Calculation of density profiles for our system using the equation of state of Hall [10] shows that we might cover the range of volume fractions from 0.22 to 0.54. This is the highest range estimation since it assumes the equilibrium situation. Considering that the sample is not at equilibrium the actual concentration

range is smaller. But even for the highest range estimation the SESANS signal would be indistinguishable (within actual error bars) from the case of a uniform concentration corresponding to some effective average of the distribution.

After 5 months of rest the sample became visibly homogeneous within a single colloidal phase with clear boundary between the colloid and pure solvent on top. The top part of colloid had blue reflections of visible light. The result of measurements at this final stage are represented in fig. 6.5. The top and the bottom curves in fig. 6.5 correspond to the top and the bottom part of the sediment. Saturation levels being functions of volume fraction are the same for the top part and the bottom part of the sample, which implies that the volume fraction of colloid does not change with the height. This fact suggests that the sample reached its maximum packing fraction of 0.58 ± 0.02, which is less than the ideal close packed volume fraction 0.74. The sedimentation profile directly measured by light scattering [3] showed that the maximal experimental volume fraction of hard sphere colloid is about 0.62 and compressibility at this concentration goes up much faster than for the ideal hard sphere system. The calculated curves for random hexagonal close packed structure [35], which is expected in case of hard spheres [21], and for a glass are superimposed on the experimental data in both graphs to show the evidence that the top part of the sample develops much more pronounced crystalline ordering than the bottom part even being at the same concentration.

We note a significant difference between the nearest-neighbour distance in the crystalline (2x160 nm = 320 nm) and the glass (2x149 nm = 298 nm) parts of the sediment, which are obtained from the fit. This difference cannot be accounted for by gravitational compression of the sediment since the gravitational length l_g is much larger than the size of the particles R (see above). We assign this difference to the colloid polydispersity [14, 13], which can drastically reduce the crystal compressibility [34]. In a glass the particle-particle positional correlations extend only over a few shells formed by the neighbouring particles. The structure is then mostly determined by the local environment and the average particle separation is governed by the average particle size. In the crystal, on the contrary, the positional order runs throughout the whole crystallite and the lattice period should be the same throughout [20, 22]. To adapt to the fluctuations in the sphere diameter, the crystal should then accept a lattice with a period, which is determined by the size of the largest particles.

The discrepancy between the solid line and the experimental data in the bottom graph of the fig. 6.5 may by attributed to a small fraction of dumbbells, formed by irreversibly aggregated particles.
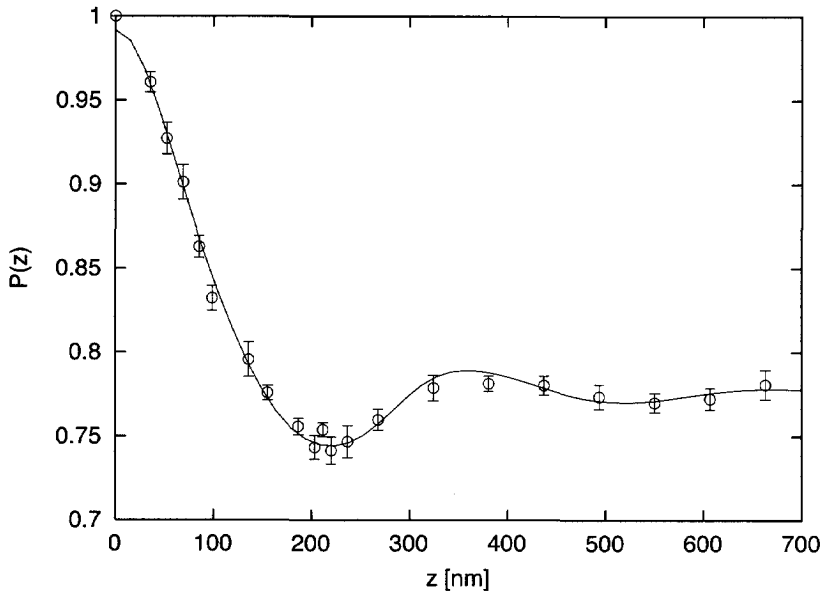
Figure 6.4: Concentrated suspension of hard spheres. The line is the calculation for the Percus-Yevick solution for a hard sphere liquid with $\phi_V = 0.32$ and $R = 149$ nm.
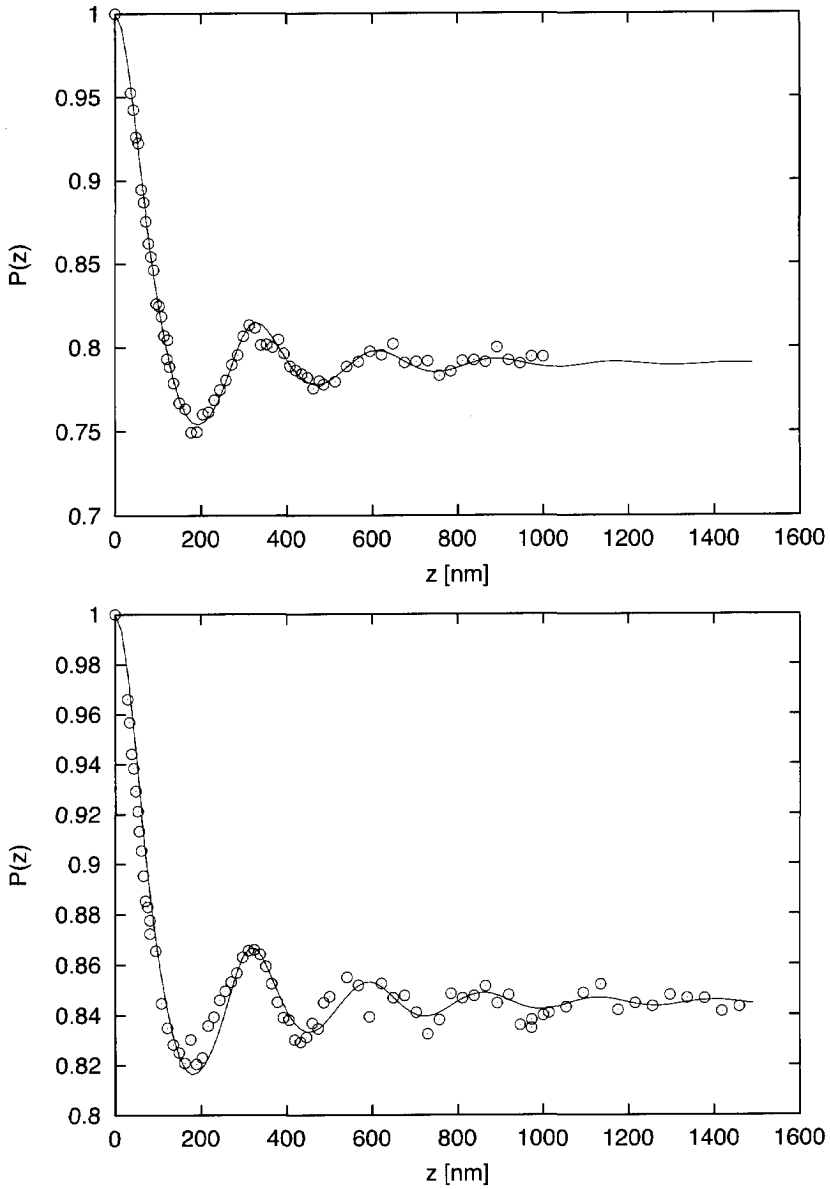
Figure 6.5: The solution from fig.6.5 after 2 weeks at rest. The top graph corresponds to the top of the sediment. The lower graph corresponds to the bottom of the sediment. Lines: Percus-Yevick solution for a hard sphere liquid with $\phi_V = 0.4$ (top) and $\phi_V = 0.5$ (bottom). $R = 149$ nm.
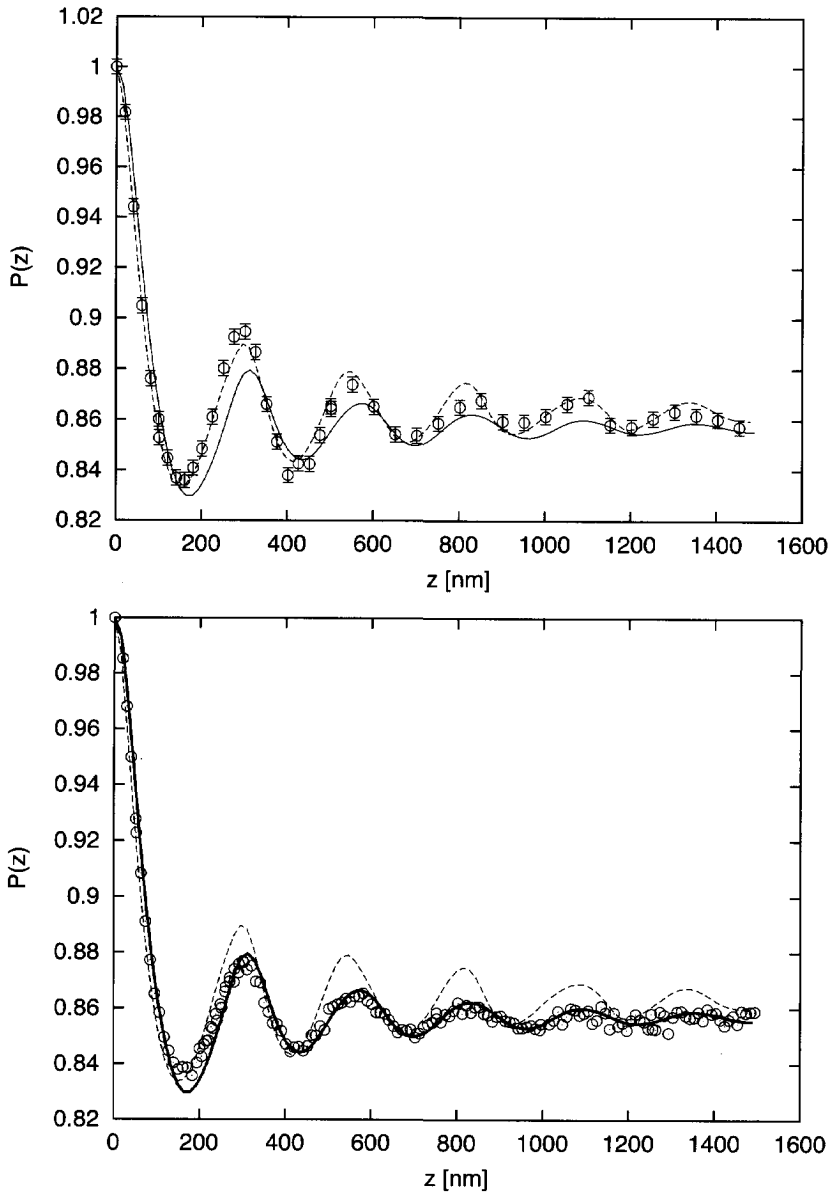
Figure 6.6: The solution from fig.6.5 after 5 months at rest. The top graph corresponds to the top of the sediment. The lower graph corresponds to the bottom of the sediment. Solid lines - Percus-Yevick equation with Henderson-Grundke correction for $\phi_V = 0.58$ and $R = 149$ nm. Dotted lines - random hexagonal close packed structure with distance between neighboring spheres 320 nm. Packing of spheres corresponds to $\phi_V = 0.58$.

Chapter 7

Aggregates

7.1 Sample preparation

Polystyrene uniform micro-spheres with a radius of 25 nm were used to pre-
pare the concentrated colloidal suspension. The source was a solution of such
spheres in H_2O, 10 % concentration, manufactured by Bangs Laboratories,
Inc., Indiana, USA (www.bangslabs.com). This solution was dried out and
then again dissolved in D_2O. The purpose of using D_2O as a solvent was
to increase the scattering length contrast of the suspension and to increase
the transmission. After dilution in D_2O to 20% solid content by volume the
mixture was intensively shaken and then put in ultrasonic bath for 2 hours.
Immediately after this process phase separation occurred. The mass density
of polystyrene spheres is 1.05 g/ml. The density of D_2O is 1.11 g/ml, which is
higher than the density of
polystyrene spheres. The bottom part of the sample was homogeneous
suspension of milky white color while the top part consisted of macroscopic
pieces of solids with sizes visible by naked eye. The solid content was in
equilibrium with homogeneous suspension. This equilibrium was visibly stable
and the boundary between these two phases did not change its position during
2 months. The whole sample was in a rectangular cell made of optical glass and
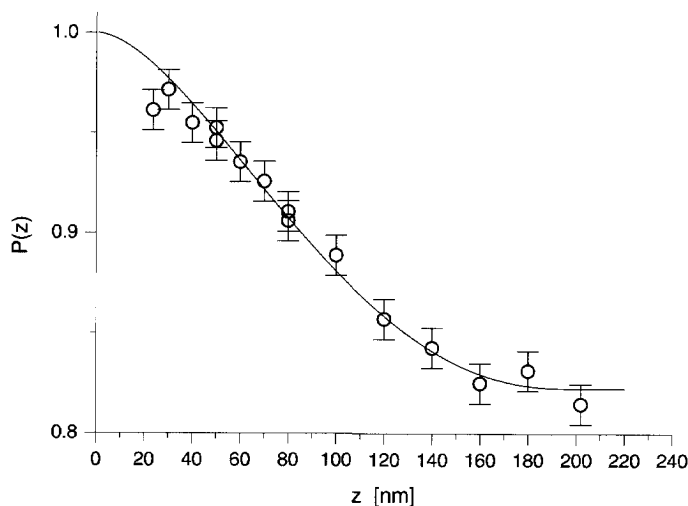with a size of 45mm (height) by 12.5mm (width) and thickness of 20mm. For

Figure 7.1: The symbols present SESANS-signal of a dilute solution of mono-disperse polystyrene spheres with a radius of R=100 nm. The drawn line is the calculated signal according to the parameters of the solution.

the scattering length density ρ of the constituents we took [12] for polystyrene $1.42 \cdot 10^{14} \mathrm{m}^{-2}$ and for D_2O $6.38 \cdot 10^{14} \mathrm{m}^{-2}$. The scattering length contrast was $4.96 \cdot 10^{14} \mathrm{m}^{-2}$.

7.2   Measurements

The measurements on the dilute solution [2] are shown in Fig. 7.1 as a reference for the concentrated system. One observes directly the size of the particle from the measured correlation function $G(z)$. The measurement agrees well with the calculated signal with (3.12) using the known parameters of the solution.

7.3   Interpretation

The constant level of polarisation of 63 % in Fig 7.2 is reached at length scales of about 1200 nm. Since the elementary unit in our system is a spherical particle of 50 nm diameter there must be clusters of such particles with a size not exceeding 1200 nm. The SESANS signal has a minimum around 700 nm, which is a sign of a repulsive potential [31] between clusters. Repulsion is a
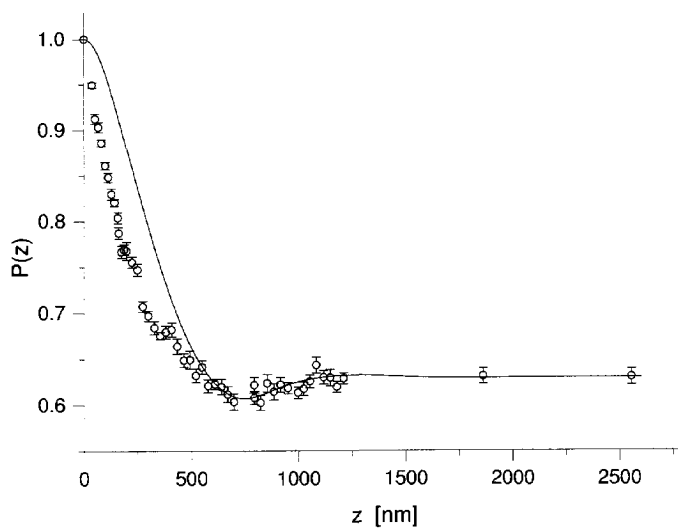
Figure 7.2: The symbols present SESANS-signal of a concentrated solution of mono-disperse polystyrene spheres with a radius of R=25 nm. The drawn line is the calculated signal for 10% volume solution of spheres of R=450 nm interacting as hard spheres.

result of hard-sphere behaviour, which in pure form can be seen at distances $z \geq 600$ nm (see fitting curve in Fig 7.2). But the fitting curve does not follow the measurement for $z \leq 600$ nm.

If we have smaller aggregates in addition to bigger ones the SESANS signal for such aggregates has a steeper slope and is cut off at smaller z values. Presence of smaller structures leads to faster decay of the resulting SESANS signal and has as a consequence a more drastic drop in polarization compared to the case of only large aggregates.

There are 2 peak-like features at about 200 nm and 400 nm which we believe correspond to internal structure of aggregates. These features reproduced exactly on our old setup, therefore we are sure that they are not an instrumental artifact. These maxima suggest that we are dealing with crystalline-like ordering which is a balance of strong repulsion and attraction. Strong attraction balanced by hard sphere repulsion leads to the appearance of peaks for $z \leq 500$ nm which could be due to sticking process which particles might undergo during drying.

Since we are dealing neither with isolated spheres nor with perfect colloidal crystals we have a big number of parameters involved in modelling the structure. A good alternative in that case would be extraction of pair correlation function. The best approach in the way of interpretation of such systems is being currently developed.

Chapter 8

Charged colloids: possibilities of attractive forces

Here we present the measurements on charge stabilized collidal suspensions. We have observed the local colloidal structure directly in real space. We consider the measurements on charged colloids in the frame of "like-charge attraction" controversy and show the advantage of SESANS' real-space domain for straightforward interpratation of the results.

8.1 The targeted problem

Charge-stabilized colloids consist of colloidal particles having easily dissociatiating surface groups. They release counterions into a solvent and become macroions. Besides counterions there can be salt ions present in a solvent. The interaction between such macroions immersed in ionic medium was claimed to be correctly described by DLVO potential since many years ago [33, 4]. Disregarding van der Waals interaction, which does not play a role in our case, this potential is repulsive and has a screened Coulombic form. However during the last two decades there were experimental studies on charge stabilized colloids inconsistent with the DLVO potential. These results suggested the presence

of attractive interaction between macroins. To explain this attraction a different theoretical approach was developed, which resulted in the Sogami potential [28]. Unlike the DLVO potential, the Sogami potential has a long range attractive tail (see Fig.1, top graphs). An overview of this problem can be found in [5]. Depending on the potential, the colloid would develop different structures. With a purely repulsive potential, such as DLVO, macroions prefer to stay at a maximum possible distance from each other. Due to steric limitations it is limited by the average distance $l = n^{-\frac{1}{3}} = \sqrt[3]{\frac{4\pi}{3\varphi}}$ between particles. It depends on the particle's concentration n (corresponding volume fraction φ) only. The DLVO potential yields a structure, which is very similar to that of an 'effective hard-spere' structure. The latter is a structure formed by spheres surrounded by imaginary concentric hard sphere shells of bigger radius, impenetrable for other shells (see dashed line on fig.8.1). If the macroions interact via Sogami potential and the condition is such that the position of the minimum R_m of the potential is smaller than l, the particles prefer to fall in this minimum rather then to stay at the distance l from each other. This would result to a maximum in SESANS correlation function shifted to $z \approx R_m < l$ compared to pure repulsive DLVO case. On a bigger scale it would lead to the development of the regions with high density coexisting with voids (see bottom graphs on fig.8.1) [1]. On the SESANS correlation function it would be seen as a "stair-like" structure, where the probability to find closer particles is higher, and the correlation with remote particles is lower. Both potentials contain the Debye length as a parameter representing the characteristic interaction length between the macroions. The Debye length is due to the shielding effect of simple ions in the solvent. The increase of salt concentration increases the shielding effect, decreases the Debye length and shifts R_m towards smaller distances. The variation of the potential upon salt concentration reflects on the structure. The real-space domain of SESANS allows straightforward interpretation of these structures unlike conventional reciprocal space scattering techniques.

8.2   Experimental results and discussion

We used silica spherical particles of a radius $R = 118$ nm, originally suspended in regular (nondeuterated) ethanol. To increase the scattering contrast, a part of the regular ethanol was substituted by deuterated one. The volume fraction of silica particles was $\varphi = 0.086$. A part of that suspension with high salt concentration (sample 1) was used to prepare the other two samples: sample 2 with low salt concentration and a salt free sample 3. As seen on the fig.8.2

the structure of the sample 3 is almost indistinguishable from that of the 'effective hard-sphere'. This structure is formed by the particles effectively repulsing each other. If the interaction was of Sogami type then the case corresponds to the condition $R_m > l$, which is expected in salt-free case for our colloid. In case of high salt concentration (fig.8.2, sample 1) the interaction is considerably screened by salt ions. If we had only strongly screened repulsion, we would expect the structure similar to that of hard spheres at the same volume fraction (fig.8.2, top, dashed line). The only structural feature would be the minimum on SESANS curve due to excluded volume. On the experimental curve (fig.8.2, top) we observe the nearest neighbour at a distance $z \approx 300$ nm. The appearance of such strongly correlated neighbours is most likely due to attraction. The intermediate sample 2 (fig.8.2, middle) shows the 'stair-like' structure expected for Sogami potential with the first neighbour at $z < l$.

With SESANS we have shown that the structure of charged colloids is consistent with the presence of attractive forces.
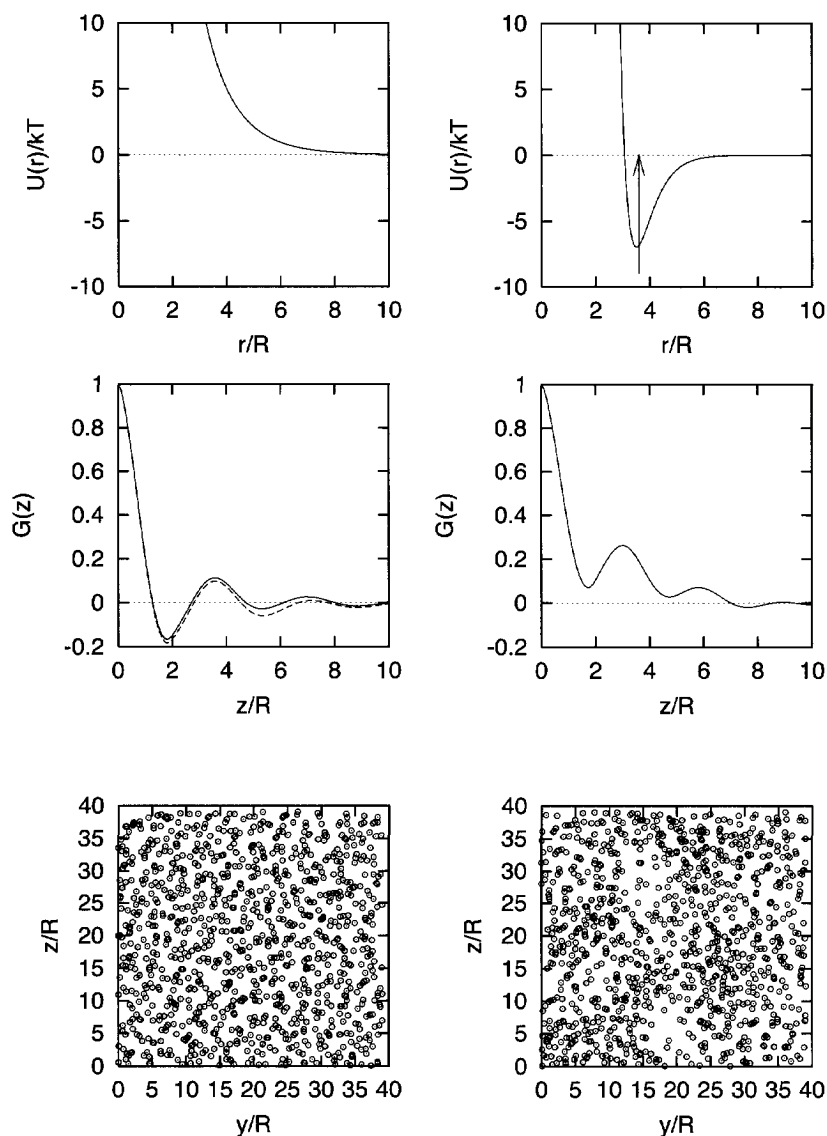
Figure 8.1: Top: DLVO (left) and Sogami (right) potentials. The arrow represents the maximum average distance l between particles. Middle: $G(z)$ for the above two potentials as a result MC simulations. The dashed line represents equivalent 'effective hard-sphere' structure. Bottom: projection of MC volume along x-axis for both potentials respectively.
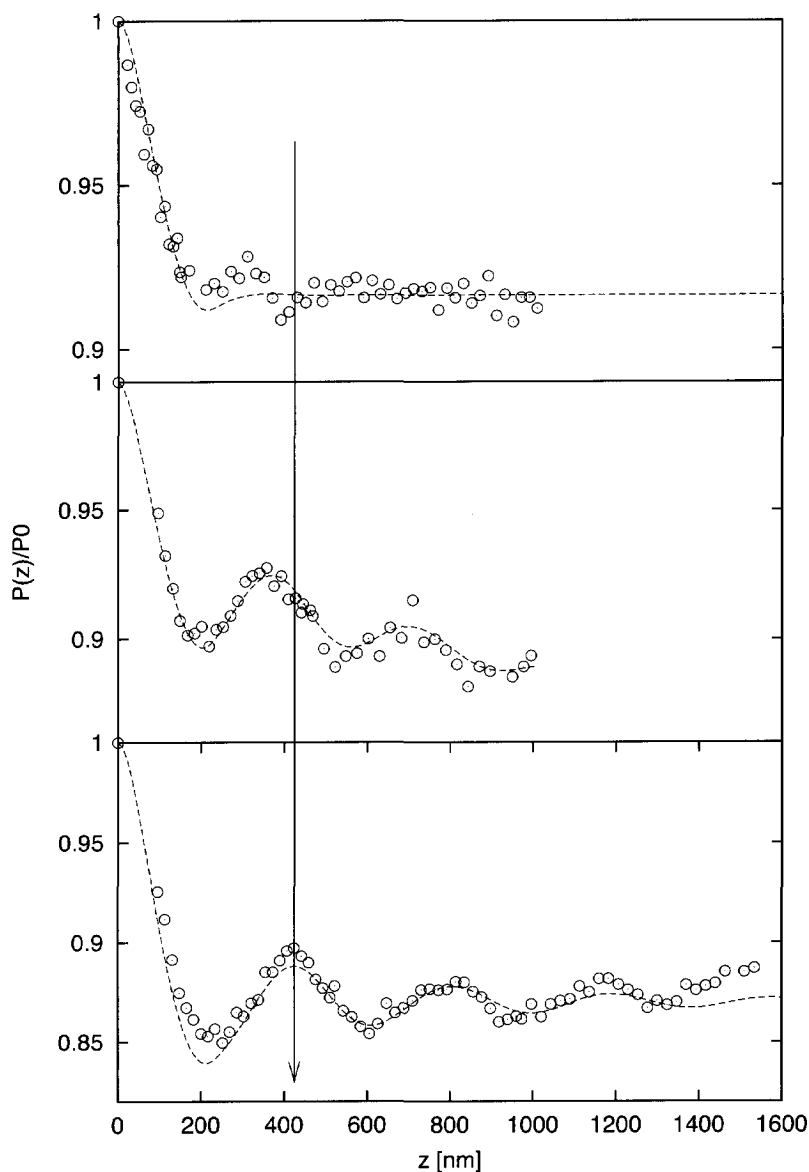
Figure 8.2: SESANS measurements on silica colloid. Top: sample 1, dashed line corresponds to hard spheres of the same φ. Middle: sample 2, dashed line is MC simulation with attractive potential. Bottom: sample 3, dashed line is 'effective hard-sphere' fit. The arrow represents the maximum average distance l between particles.

Chapter 9

Charged colloids: the role of the effective excluded volume

Based on
Timofey Kruglov, Wim G. Bouwman and Jeroen Plomp.
Correlation function of the effective excluded volume and its application to charged colloids studied by Spin-echo Small-angle Neutron Scattering.
in preparation.

We introduce the correlation function and length of the effective excluded volume and calculate it analytically for spherical particles. We show how structure of charged colloids measured by Spin-Echo Small-Angle Neutron Scattering can be interpreted in terms of this function. We compare the role of the excluded volume for hard sphere and charged colloids. We show that for charged colloids the effect of the excluded volume greatly overshadows the effect of the rest of the structure in terms of scattering probability.

9.1 Correlation function, length and scattering probability

Correlation function of the excluded volume for a system of spherical particles was introduced in [17]. It was shown that the conventional correlation function can be decomposed into three components:

$$\gamma(r) = \gamma_{auto}(r) - \varphi\gamma_{excl}(r) + \varphi\gamma_{struct}(r) \tag{9.1}$$

where $\gamma_{auto}(r)$ is auto correlation function, φ is a volume fraction of spheres,

$$\gamma_{excl}(r) = \int_0^2 \gamma_{ovl}(r,a)3a^2da \qquad (9.2)$$

is the correlation function of the excluded volume and

$$\gamma_{struct}(r,g) = \int_2^\infty \gamma_{cross}(r,a)(g(a)-1)3a^2da \qquad (9.3)$$

is the structural correlation function, $\gamma_{cross}(r,a)$ is a cross correlation function calculated in [7]), $g(a)$ is a pair correlation function $\gamma_{ovl}(r,a)$ is a correlation function of two overlapping spheres with a distance $0 < a < 2$ between their centers. The closest distance the two hard spheres can approach each other is 2 (all spatial variables are measured in spheres' radius units). Therefore all possible overlaps at distances $0 < a < 2$ are integrated yielding the correlation function of the excluded volume (9.2). $\gamma_{cross}(r,a)$ is a cross correlation function of two spheres separated by a distance $2 \geq a < \infty$ between their centers. Integrated with the probability $g(a) - 1$ they yield the structural correlation function The range of validity of $\gamma_{ovl}(r,a)$ and $\gamma_{cross}(r,a)$ is shown in fig.9.1. Strictly speaking, the excluded volume is also a part of a structure, but here we separate it as a first approximation. We separate structural correlations inside and outside of the excluded volume. This is defined by spheres' diameter 2, which is an upper and lower limits of integration in (9.2) and (9.3) respectively. Now suppose spheres interact via soft repulsive potential, for instance a screened Coulombic (see fig.9.2). It can be approximated with an *effective hard sphere* potential. Instead of a real soft potential each sphere is concentrically surrounded by an imaginary impermeable shell of a bigger *effective* diameter $b > 2$. While bare spheres still remain hard spheres with the diameter 2, which is the upper limit of integration in (9.2) and (9.3) the *efective* hard sphere diameter extends to $b > 2$. This *effective* hard sphere effect can be separated from the rest of the structure by rewriting (9.1) in a following way:

$$\gamma(r) = \gamma_{auto}(r) - \varphi\gamma_{excl}(r,b) + \varphi\gamma_{struct}(r,g) \qquad (9.4)$$

where the *correlation function of the effective excluded volume* is:

$$\gamma_{excl}(r,b) = \gamma_{excl}(r) + \int_2^b \gamma_{cross}(r,a)3a^2da \qquad (9.5)$$

and a structural part becomes (compare to (9.3))

$$\gamma_{struct}(r, g) = \int_b^\infty \gamma_{cross}(r, a)(g(a) - 1)3a^2 da \qquad (9.6)$$

$\gamma_{excl}(r, b)$ now depends on the effective excluded diameter b. The analytical expression for this function is given in app.9.6.1

If a small-angle approximation is applied one gets a (Spin-Echo) Small-Angle correlation function, which is a projection of conventional correlation function along a neutron beam (x-axis) [15, 18]:

$$G(z) = \int_{-\infty}^\infty \gamma(\sqrt{x^2 + 0^2 + z^2})dx = 2 \int_z^{+\infty} dr \frac{\gamma(r)r}{\sqrt{r^2 - z^2}} \qquad (9.7)$$

The same decomposition (9.4) can be made for the SESANS correlation function:

$$G(z) = G_{auto}(z) - \varphi G_{excl}(z, b) + \varphi G_{struct}(z, g) \qquad (9.8)$$

where $G_{auto}(z)$ is given in [15], $G_{excl}(z, b)$ is given in the app. 9.6.2 and

$$G_{struct}(z, g) = \int_b^\infty G_{cross}(z, a)(g(a) - 1)3a^2 da \qquad (9.9)$$

where $G_{cross}(r, a)$ is calculated in [18].

The same can be done for correlation length:

$$\xi = \int_{-\infty}^{+\infty} \gamma(r)dr = G(0) = \xi_{auto} - \varphi\xi(b) + \varphi\xi_{struct}(g) \qquad (9.10)$$

where

$$\xi_{excl}(b) = \int_0^{b+2} \gamma_{excl}(r, a)dr \qquad (9.11)$$

is given in the app. 9.6.3 and

$$\xi_{struct}(g) = \int_b^\infty \xi_{cross}(a)(g(a) - 1)d(a^3) \qquad (9.12)$$

(see fig.9.4) where

$$\xi_{cross}(a) = 2 \int_{a-2}^{a+2} \gamma_{cross}(r, a)dr \qquad (9.13)$$

is a cross correlation length of two spheres separated by a distance a between their centers.

The directly measured quantity in SESANS is polarization of a neutron beam passed though a sample

$$P(z) = e^{G_c(z) - G_c(0)} \tag{9.14}$$

where for a system of spherical particles

$$G_c(z) = \varphi (\Delta \rho)^2 \lambda^2 t R G(z) \tag{9.15}$$

where $\Delta \rho$ is a contrast, λ is a neutron wavelength, t is a sample thickness, R is a radius of a spheres. $G_c(0)$ is a total cumulative scattering probability and is proportional to the correlation length

$$G_c(0) = \varphi (\Delta \rho)^2 \lambda^2 t R \xi \tag{9.16}$$

SESANS measures scattered beam on top of the transmitted part $P(\infty)$. If we subtract it we get only the scattered part

$$\Delta P(z) = P(z) - P(\infty) \tag{9.17}$$

The total true scattering probability is [18]

$$\Delta P(0) = 1 - e^{G_c(0)} \tag{9.18}$$

9.2   Structure versus excluded volume

The correlation length is proportional to the total apparent scattering probability. It allows us to estimate the contribution to scattering of the effective excluded volume and the structural arrangement of the particles by comparing ξ_{excl} and ξ_{struct}. If a volume fraction of particles is φ and the *effective* diameter is b then the *effective* volume fraction (volume fraction of impermeable shells) is $\varphi_{eff} = \varphi \left(\frac{b}{2} \right)^3$.

Let us fix the size and volume fraction of the excluded volume and shrink the size of the spheres inside it as depicted in fig. 9.5. The correlation length will change accordingly as plotted in fig.9.6. The rightmost limit corresponds to $\varphi = \varphi_{eff} = 0.27$ and $b = 2$. The ratio $\frac{\xi_{excl}}{\xi_{struct}} = \frac{0.48}{0.10}$ equals to the ratio of the total apparent scattering probabilities (per particle) of those two effects.

If we shrink the real particle size, which will lead to the decrease of their real volume fraction φ, we see that the effect of the structural arrangement
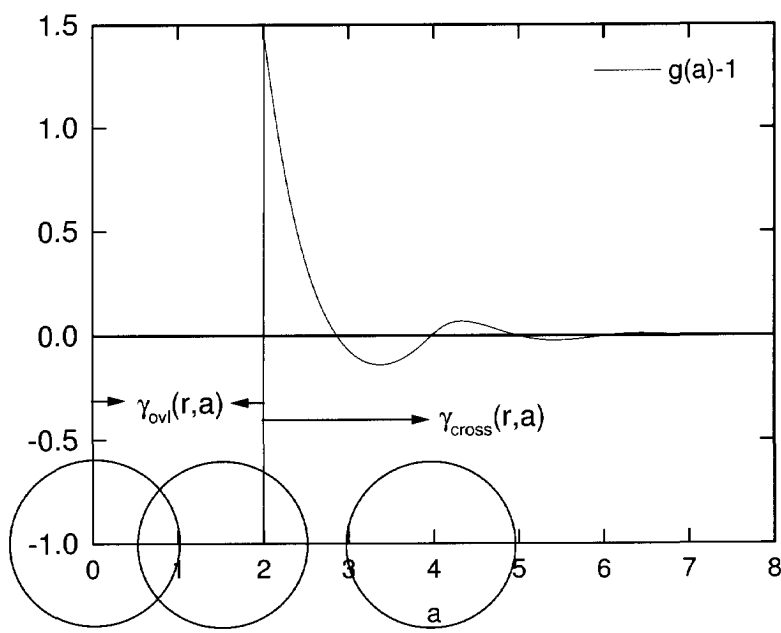
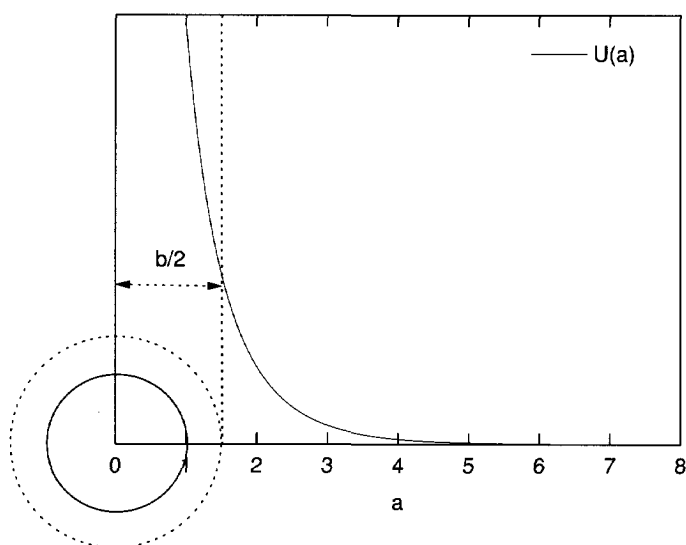Figure 9.1: Domain of definition of $\gamma_{ovl}(r,a)$ and $\gamma_{cross}(r,a)$.

Figure 9.2: Screened coulombic potential and its effective hard sphere equivalent.

given by ξ_{struct} disappears much faster than the effect of the excluded volume given by ξ_{excl}. At $\varphi = 0.01$ the total scattering probability of the structural arrangment accounts to only one percent of that of the effect of the effective excluded volume.
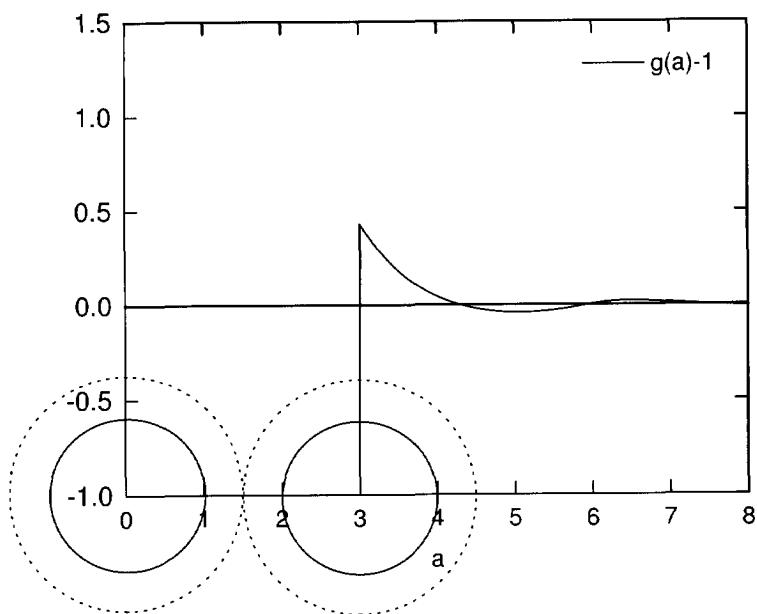
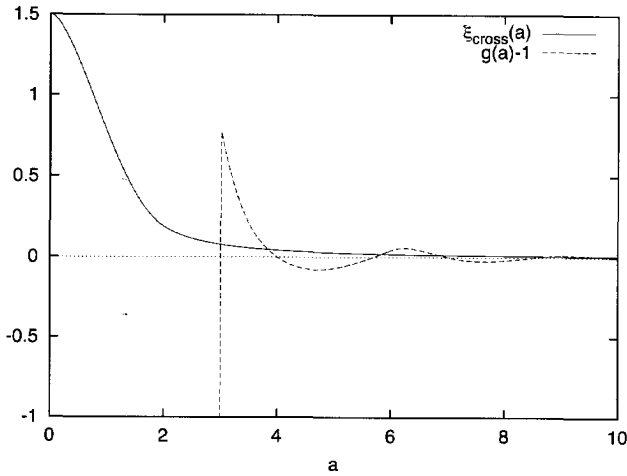Figure 9.3: Excluded volume for effective hard spheres with $b = 3$.

Figure 9.4: $\xi_{cross}(a)$ and $g(a) - 1$ to be integrated according to (9.12) with $b = 3$

9.3   Hard sphere colloids

9.3.1   Sample

As a source of particles we used sterically stabilized silica spheres suspended in cyclohexane. The initial solution was dried under low (≈ 0.1 atm) pressure during 12 hours. Dry particles were then redispersed in deuterated cyclohexane. Directly after redispersion the sample appeared macroscopically homogeneous. These particles are known to be redispersed easily after drying. A deuterated solvent was used in order to maximize the scattering contrast and minimize incoherent scattering. We prepared a solution in a 5 mm thick cell (the neutron path length), 10 mm wide and 40 mm high. The thicknesses of samples were chosen such as to give considerable depolarisation, but not close to zero saturation level. The sample was illuminated by the neutron beam framed by a cadmium diaphragm 8.5 mm high and 7.5 mm wide which was mounted immediately in front of the cell.

9.3.2   Results

The radius of the particles $R = 149$ nm was determined using the dilute suspension of the same colloid [16]. The scattering density of silica 2.35×10^{10}
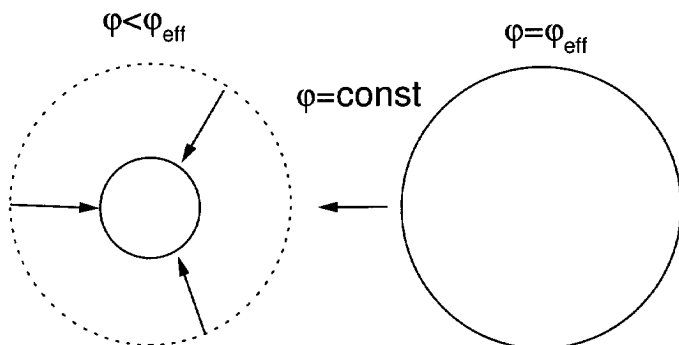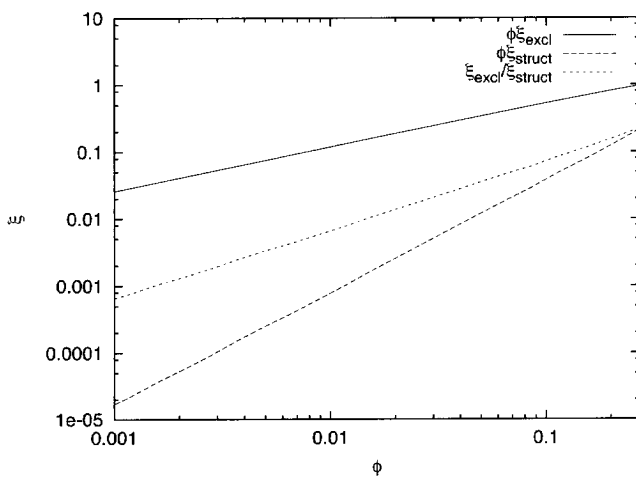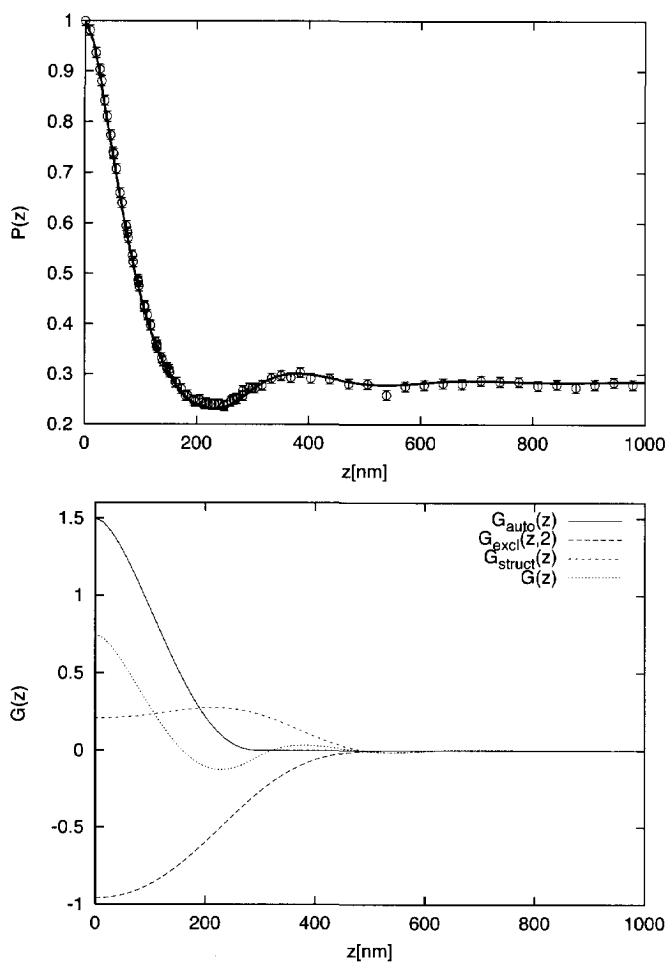
Figure 9.5: Shrinking of real sphere inside impermeable shell.

Figure 9.6: ξ_{excl} and ξ_{struct} as functions of volume fraction for effective hard sphere liquid with $\varphi_{eff} = 0.27$.

Figure 9.7: Hard sphere colloid at $\varphi = 0.27$.

cm^{-2} was determined as a result of fitting, which is almost the same as the theoretical value 2.4×10^{10} cm^{-2}. For deuterated cyclohexane we used $\rho_{C_6 D_{12}} = 6.7 \times 10^{10}$ cm^{-2} [12]. In order to calculate the structural part of $G(z)$ we used Percus-Yevick pair distribution function. The volume fraction of the particles $\varphi = 0.27$ was determined by fitting the experimental curve (see fig.9.7, top). $G(z)$ obtained as a result of fitting $P(z)$, consists of the three components (fig.9.7, bottom). $G_{auto}(0)$, $G_{excl}(0)$ and $G_{struct}(0)$ and give the length of respective correlations in terms of the particles' radius. $G_{auto}(0) = \xi_{auto} = \frac{3}{2}$ is a single sphere's correlation length which does not depend on interactions. In general, it is a function of a particle's shape and density. $-G_{excl}(0) = \varphi \xi_{excl}$ is a linear function of particle's concentration, where $\xi_{excl}(2) = \frac{36}{35}(9 - 8\ln(2)) \approx 3.55$ is the correlation length of the excluded volume of a single sphere. $G_{struct}(0) = \varphi \xi_{struct}$, where ξ_{struct} (see (9.12)) is defined by mutual arrangement of the spheres. Multiple scattering for that sample was very strong, yielding the cumulative scattering probability $G_c(0) = 1.2$ and true scattering probability $\Delta P(0) = 0.7$, which is the total depolarization level in fig.9.7.

The ratio $\frac{G_{struct}(0)}{G_{excl}(0)} = 0.2$ corresponds to the rightmost point of the fig.9.6 where $\varphi = \varphi_{eff} = 0.27$. For pure hard-sphere interaction at this concentration the effect of the structural ordering is comparable to the effect of the excluded volume.

$P(z)$ bears structural information which allows straightforward interpretation. The initial decay in fig. 9.7 coresponds to the correlations within a single sphere. The subsequent minimum around 250 nm corresponds to the excluded volume effect. The maximum at 400 nm corresponds to the first nearest neighbour. Subsequent correlations are barely visible and the curve reaches the saturation.

9.4 Charged colloids

9.4.1 Sample

Unlike sterically stabilized hard sphere colloids, charged ones can not be re-dispersed after complete drying due to the irreversible aggregation (which was confirmed by SESANS). They were prepared in a following way. The stock solution [29] of silica spheres with $R = 118$ nm in $C_6 H_{12}$ was left to sediment for several weeks. Then the sediment was put into $C_6 D_{12}$ (sample 3). Part of the sample 3 was left to sediment for several weeks, then the supernatant

solvent was removed and substituted again by pure C_6D_{12} (sample 1). Part of the sample 1 was left to sediment for several weeks again. The supernatant solvent was removed and substituted by pure C_6D_{12} (sample 2). As a result of these procedures the three samples had characteristics summarized in the first five columns of the table 9.4.2. Samples 1 and 2 were put into cells 10mm thick (neutron beam path), 20 mm wide and 40 mm high. The illuminated area was restricted by a diaphragm 18 mm wide and 8 mm high. Sample 3 was in a cell 10 mm thick, 10 mm wide and 40 mm high, the diaphragm was 7.5 mm wide and 8.5 mm high.

9.4.2 Results

The screened Coulombic potential [4, 33]

$$U(r) \sim \frac{e^{-\kappa r}}{r}$$

is believed [1] to describe interactions in charged colloids. The Debye length κ^{-1} defines the characteristic range of the interaction. If we had only pairwise interactions the excluded diameter would apparently be proportional to the Debye length $b \sim \kappa^{-1}$. The Debye length is determined by the concentration of ions in a solvent. At the same time a is affected by the presence of neighbours, which decrease the excluded diameter due to steric limitations. An upper limit is $b \sim \langle l \rangle = \sqrt[3]{\frac{4\pi}{3\varphi}}$, where $\langle l \rangle$ is the average interparticle distance. The competition of these two factors defines the resulting b. The ion concentration, which greatly affects κ^{-1}, might differ from sample to sample and was not controlled precisely. The effects of salinity on the potential and thus on the structure are outside the scope of this paper.

Estimation of the effects of the excluded volume and mutual ordering can be made from the comparison of $G_{excl}(0)$ and $G_{struct}(0)$. In all three cases $G_{struct}(0)$ is negligibly small compared to $G_{excl}(0)$. This can be understood looking at lower volume fractions on fig.9.6. The parameters characterizing the samples are summarized in the table 9.4.2. The effective volume fraction (volume fraction of the impearmeable shells) is obtained using

$$\varphi_{eff} = \varphi \left(\frac{b}{2} \right)^3$$

Here the real space domain of SESANS demonstrates its advantage in the ease of result interpretation of local structure. The initial decay corresponds to

---

[1]It is a still debated issue, but it is outside of the scope of this paper
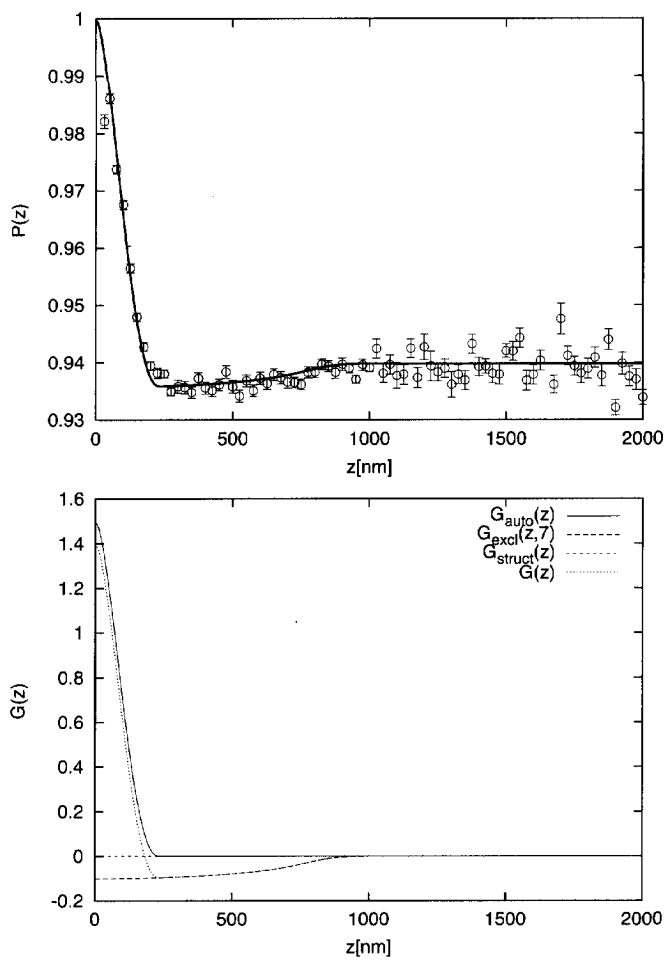
Figure 9.8: Charged colloid at $\varphi = 0.0072$:
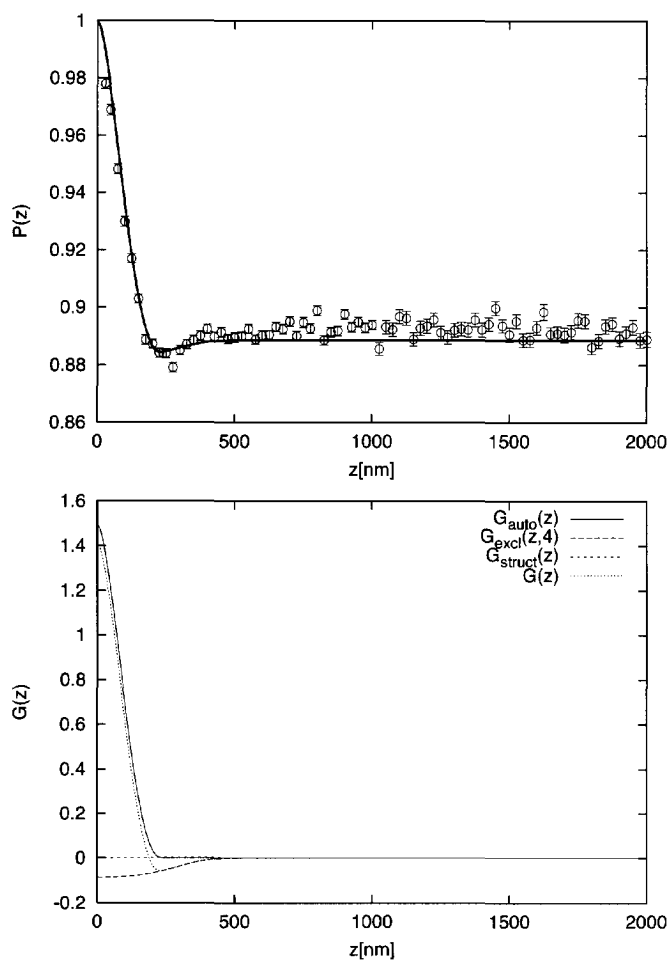
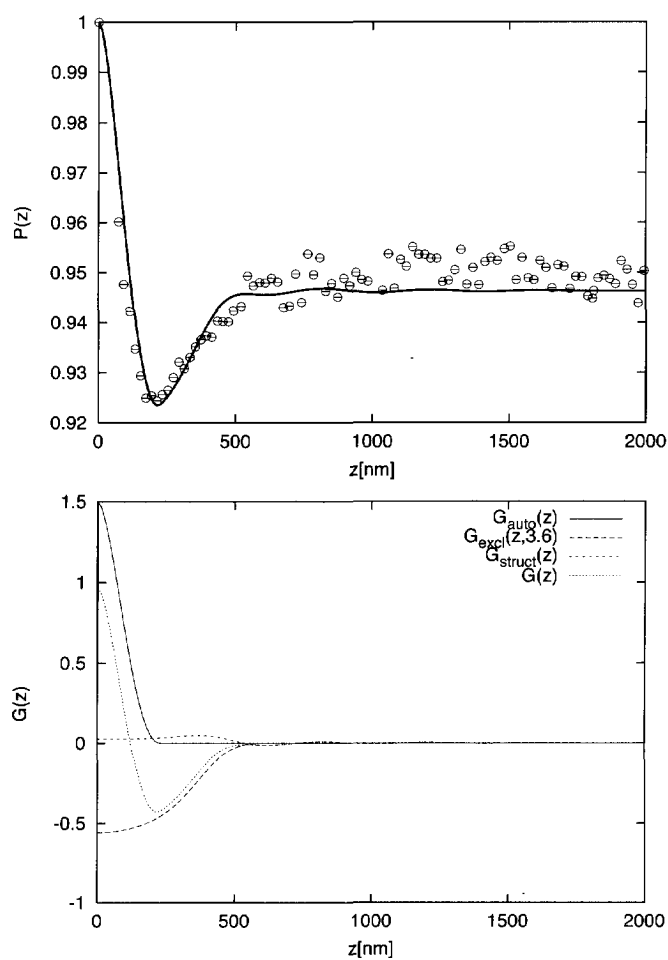Figure 9.9: Charged colloid at $\varphi = 0.015$:

Figure 9.10: Charged colloid at $\varphi = 0.08$:

Table 9.1: Charged colloids.

smpl N	φ	D:H %:%	$\rho_{solvent}$ $\times 10^{10} \frac{1}{cm^2}$	$\Delta\rho$ $\times 10^{10} \frac{1}{cm^2}$	$\frac{\langle l \rangle}{2R}$	$\langle l \rangle$ nm	$\frac{b}{2R}$	$b/2$ nm	φ_{eff}
1	0.0072	95.3:4.7	5.84	3.44	4.1	970	3.5	826	0.31
2	0.015	92.8:7.2	5.67	3.27	3.2	760	2	472	0.12
3	0.08	60:40	3.57	1.17	1.84	435	1.8	425	0.47

the correlations within a single sphere, the subsequent minimum is the effect of the excluded volume. In case of the sample 3 it is much more pronounced than in the case of hard spheres even though the volume fraction is 4.5 times lower. The nearest neighbour is virtually invisible.

9.5   Conclusion

SESANS allows straightforward interpretation of structure due to its real space domain. The (SESANS) correlation function and length of the effective excluded volume is introduced and calculated analytically for spheres as a function of the excluded radius. The separation of the excluded volume correlations as a first structural approximation allows to treat the experimental results on charged colloids regardless of a particular interaction potential. We obtain the excluded radius by a direct fit. The correlation length is proportional to the cumulative scattering probability on the corresponding structural features. For a dilute charged colloid the effect of the excluded volume greatly overshadows the effect of the rest of the structure.

9.6   Appendices

9.6.1   Correlation function of the effective excluded volume

$$\gamma_{excl}(r,b) = \begin{cases} 1 & \text{if } 0 \leq r \leq b-2 \\ \gamma_p(r,b) + \gamma_n(r,b) & \text{if } b-2 \leq r \leq b \\ \gamma_p(r,b) - \gamma_n(r,b) & \text{if } b \leq r \leq b+2 \\ 0 & \text{if } b+2 < r \end{cases}$$

where

$$\gamma_p(r, b) = \frac{1}{2} + \frac{b^3}{2} - \frac{9}{35r} + \frac{3b^2}{r} - \frac{3b^4}{16r} - \frac{3r}{10} - \frac{3b^2 r}{8} + \frac{r^3}{16}$$

$$\gamma_n(r, b) = -\frac{9b^4}{32} + \frac{b^6}{64} + \frac{3b^5}{40r} - \frac{3b^7}{1120r} + \frac{3b^3 r}{8} - \frac{3b^5 r}{80} - \frac{3b^2 r^2}{16} + \frac{3b^4 r^2}{64} - \frac{b^3 r^3}{32} + \frac{3r^4}{160} + \frac{3b^2 r^4}{320} - \frac{r^6}{2240}$$
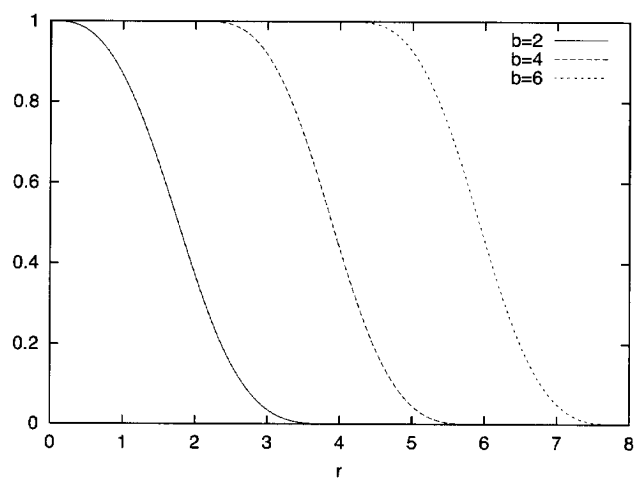
Figure 9.11: $\gamma_{excl}(r, b)$ for $b = 2$, $b = 4$ and $b = 6$.

9.6.2 (SE)SANS correlation function of the effective excluded volume

$$G_{excl}(z, b) =$$

$$
\begin{cases}
\begin{aligned}
& 2\sqrt{(b-2)^2 - z^2} \\
& -G_p(z, b, b-2) + G_p(z, b, b+2) \\
& -G_n(z, b, b-2) + G_n(z, b, b) \\
& +G_n(z, b, b) - G_n(z, b, b+2) && \text{if } 0 \le z \le b - 2 \\[2mm]
& -G_p(z, b, z) + G_p(z, b, b+2) \\
& -G_n(z, b, z) + G_n(z, b, b) \\
& +G_n(z, b, b) - G_n(z, b, b+2) && \text{if } b - 2 \le z \le b \\[2mm]
& -G_p(z, b, z) + G_p(z, b, b+2) \\
& -G_n(z, b, z) + G_n(z, b, b+2) && \text{if } b \le z \le b + 2 \\[2mm]
& 0 && \text{if } b + 2 \le z
\end{aligned}
\end{cases}
$$

where

$$
G_p(z, b, r) = \frac{1}{2240} \Big[7\sqrt{r^2 - z^2} \times \\
\big(320 + 320b^3 - 96r - 120b^2 r + 10r^3 + 15rz^2\big) - \\
3\big(384 - 448b^2 + 280b^4 + 224z^2 + 280b^2 z^2 - 35z^4\big) \times \\
\ln\left(r + \sqrt{r^2 - z^2}\right)\Big]
$$

and

$$
G_n(z, b, r) = \frac{1}{4480} \Big[\frac{1}{35}\sqrt{r^2 - z^2} \times \\
\big(-82200b^4 + 4900b^6 + 58800b^3 r - 5880b^5 r - 19600b^2 r^2 + \\
4900b^4 r^2 - 2450b^3 r^3 + 1176r^4 + 588b^2 r^4 - 20r^6 - \\
39200b^2 z^2 + 9800b^4 z^2 - 3675b^3 r z^2 + 1568r^2 z^2 + \\
784b^2 r^2 z^2 - 24r^4 z^2 + 3136z^4 + 1568b^2 z^4 - 32r^2 z^4 - 64z^6\big) - \\
3b^3\big(-224b^2 + 8b^4 - 560z^2 + 56b^2 z^2 + 35z^4\big) \times \\
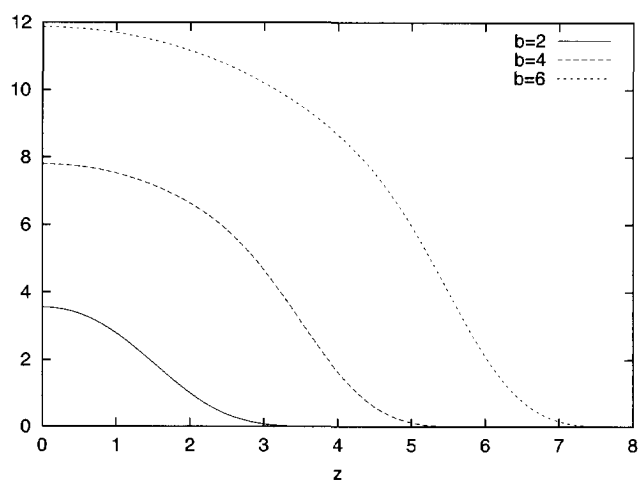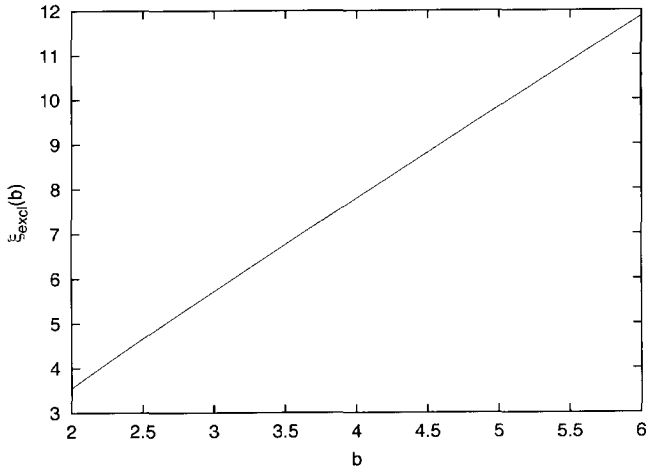\ln\left(r + \sqrt{r^2 - z^2}\right)\Big]
$$

Figure 9.12: $G_{excl}(z, b)$ for $b = 2$, $b = 4$ and $b = 6$.

Figure 9.13: $\xi_{excl}(b)$

9.6.3 Correlation length of the effective excluded volume

$$\xi_{excl}(b) =$$
$$\frac{3}{560}\left[4b(24 + 44b^2 + b^4)+\right.$$
$$(b-2)^4(b(b+2)(b+6) + 6)\ln(b-2) +$$
$$(b+2)^4(b(b-2)(b-6) - 6)\ln(b+2) -$$
$$\left.2b^5(b^2 - 28)\ln b\right]$$

Summary

SESANS technique

- Is a real-space small-angle scattering device. It measures correlations in one direction. The polarization mesured by SESANS is a fourier image of the true scattering cross section measured by conventional SANS.

- Does not suffer from multiple scattering problem unlike conventional SANS.

- Gives information about the structure of a sample in real space.

- Allows direct interpretation in terms of correlation functions.

- Due to its accessible size range fits ideally for colloidal systems.

SESANS measured quantities

- The real space formalism for the description of scattering is developed.

- Explicit relations between scattering cross section and conventional correlation function from one hand and small-angle correlation function and SESANS correlation function from the other hand are established. The SESANS' correlation function is a projection of conventional correlation function along the neutron beam.

- The general parameters such as scattering length, Guinier radius and scattering probability are calculated using SESANS correlation function.

- SESANS correlation functions are calculated for Gaussian coils, solid and hollow spheres analytically.

- The complete theory of SESANS correlation functions is developed for dense systems of spherical particles. In the framework of this formalism the following quantities are introduced:

- cross correlation function/length
- structural correlation function/length
- correlation function/length of overlapping spheres
- correlation function/length of the excluded volume

Experiment

- Measurements on hard sphere colloids show that SESANS correlation function provides information about correlations for lengths up to $1.5\mu m$ and easily takes into account multiple scattering, which was high in all measured cases. The scattering density, volume fraction and the radius of particles are determined from SESANS measurements. SESANS measurements on a hard sphere colloid demonstrate very good agreement with the theoretical curves for non-interacting spheres, a hard sphere liquid and a random hexagonal close-packed structure.

- SESANS is particulary effective to determine local structure, especially in case of aggregation or attractive interactions. Increase or decrease of correlations allows straightforward conclusions in those cases.

- The structure of charged colloids at certain conditions is consistent with the presence of attractive forces.

- Separation of the excluded volume correlations as a first structural approximation allowes to treat the experimental results on charged colloids regardless of a particular interaction potential. This approach allowes to obtain the excluded volume by direct fit.

Samenvatting

De SESANS techniek

- Is een instrument voor kleine-hoek-verstrooiing in de reële ruimte. Men kan er correlaties in één richting mee meten. De polarisatie gemeten met SESANS is een Fourier-afbeelding van de ware verstrooiings doorsnede zoals gemeten wordt met conventionele SANS.

- Heeft niet te lijden van het probleem van meervoudige verstrooiing zoals conventionele SANS.

- Geeft informatie over de structuur van een sample in de reële ruimte.

- Laat rechtstreekse interpretatie toe van de resultaten in termen van correlatiefuncties.

- Is door het bereikbare gebied van correlatielengtes ideaal geschikt voor colloidale systemen.

Grootheden gemeten met SESANS

- Er is een reële ruimte formalisme ontwikkeld voor het beschrijven van verstrooiing.

- Er zijn expliciete relaties afgeleid enerzijds tussen de verstrooiingsdoorsnede en de conventionele correlatiefunctie en anderzijds tussen de "small angle correlation function" en de SESANS correlatiefunctie. Deze functie is de projectie van de conventionele correlatiefunctie langs de richting van de neutronen.

- Uitgaande van de SESANS correlatiefunctie worden de algemene parameters berekend, zoals de verstrooiingslengte, de Guinier straal en de verstrooiingskans.

- De SESANS correlatiefuncties voor lichamen in de vorm van Gaussische kluwen, massieve en holle cylinders worden analytisch uitgerekend.

- De gehele theorie voor de SESANS correlatiefunctie is ontwikkeld voor dichte systemen van bolvormige deeltjes. In het kader van dit formalisme zijn de volgende grootheden ingevoerd:

  - de cross correlatie functie/lengte
  - de structurele correlatie functie/lengte
  - de correlatiefunctie/lengte voor overlappende bollen
  - idem voor het uitgesloten volume

Experiment

- Metingen aan harde bollen colloiden laten zien dat de SESANS correlatiefunctie informatie geeft over correlaties over afstanden tot 1.5 μm en dat de meervoudige verstrooiing - die in alle gemeten gevallen hoog was - gemakkelijk kan worden meegenomen in de analyse. Uit de SESANS metingen zijn de verstrooiingslengtedichtheid, volumefractie en de straal van de deeltjes bepaald. SESANS metingen aan harde bollen colloiden vertonen een zeer goede overeenstemming met de theoretische krommen voor niet-wisselwerkende bollen, voor een vloeistof van harde bollen en voor de random hexagonale dichtste stapeling structuur.

- SESANS is uitzonderlijk effectief in het bepalen van lokale structuur, in het bijzonder in het geval van samenklontering van deeltjes of van aantrekkende interacties. Een toe- of afname van correlaties laat rechtstreekse conclusies in deze gevallen toe.

- De structuur van geladen colloiden is onder bepaalde voorwaarden consistent met de aanwezigheid van aantrekkende krachten.

- Het concept van correlaties in het uitgesloten volume, als eerste structuurbenadering, liet toe om de experimentele resultaten aan geladen colloiden te behandelen, ongeacht een specifieke interactie potentiaal. Deze benadering maakt het mogelijk om door rechtstreeks fitten het uitgesloten volume te bepalen.

Bibliography

[1] P. V. Rajamani B. V. R. Tata, E. Yamahara and N. Ise. *Phys. Rev. Lett*, 78:2660, 1997.

[2] W.G. Bouwman, O. Uca, S.V. Grigoriev, Kraan W.H., J. Plomp, and M.T. Rekveldt. First quantitative test of spin-echo small-angle neutron scattering. *Applied Physics A Materials Science Processing*, A74:115–117, 2002.

[3] V. Degiorgio, R. Piazza, and T. Bellini. *Il Nuovo Cimento*, 16D:1091–1101, 1994.

[4] B. V. Derjaguin and L. Landau. *Acta Physicochimica*, 14:633, 1941.

[5] edited by A.K. Arora and B.V.R. Tata. *Ordering and Phase Transitions in Charged Colloids*. VCH,New York, 1996.

[6] L. A. Feigin and D. I. Svergun. *Structure analysis by small-angle X-ray and neutron scattering*. Plenum Press, New York, 1987.

[7] O Glatter. *Acta Phys. Austr.*, 52:243–256, 1980.

[8] O. Glatter and O. Kratky, editors. *Small-Angle X-ray Scattering*. New York: Academic Press, 1982.

[9] A. Guinier and G Fournet. *Small-angle scattering of X-rays*. New York: Wiley, 1955.

[10] K.R Hall. *Journal of Chemical Physics*, 57:2252–2254, 1970.

[11] J.P Hansen and I.R. McDonald. *Theory of Simple Liquids*. San Diego: Academic Press, 1991.

[12] S.M. King. *Small-angle Neutron Scattering*. John Wiley & Sons Ltd, 1999.

[13] D. Kofke and P. Bolhuis. *Phys.Rev.E,* 59:618–622, 1999.

[14] W. Kranendonk and D. Frenkel. *Molecular Physics,* 72:679–697, 1991.

[15] I.M. Krouglov, T. de Schepper, W.G. Bouwman, and M.T. Rekveldt. *Journal of Applied Crystallography,* 36:117–124, 2003.

[16] T. Krouglov, W.G. Bouwman, J. Plomp, M.T. Rekveldt, G.J. Vroege, A.V. Petukhov, and D.M.E. Thies-Weesie. *J.Appl.Cryst.,* 36:1417–1423, 2003.

[17] Timofey Kruglov. Correlation function of the excluded volume. 2005. submitted to Journal of Applied Crystallography.

[18] Timofey Kruglov. Spin-echo small-angle neutron scattering for dense systems of spheres. 2005. submitted to Journal of Applied Crystallography.

[19] F. Mezei, C. Pappas, and T. Gutberlet, editors. *Neutron Spin Echo, Lecture Notes in Physics,* volume 601. Berlin: Springer, 2003.

[20] R. Peierls. *Surprises in Theoretical Physics.* Princeton University Press, Princeton, NJ., 1979.

[21] A. Petukhov, I. Dolbnya, D. Aarts, G. Vroege, and H. Lekkerkerker. *Phys.Rev.Lett.,* 90:028304, 2003.

[22] A. Petukhov, I. Dolbnya, E. de Hoog, K. Kassapidou, G. Vroege, W. Bras, and H. Lekkerkerker. *Phys.Rev.Lett.,* 88:208301, 2002.

[23] P. N. Pusey. *Colloidal suspensions,* pages 763–942. Amsterdam: Elsevier, 1991.

[24] M.T. Rekveldt. *Nucl. Instrum. Methods Phys. Res. B,* 114:366–370, 1996.

[25] M.T. Rekveldt, W.G. Bouwman, Kraan W.H., O. Uca, S. Grigoriev, K Habicht, and T Keller. Neutron spin echo, lecture notes in physics. In Mezei et al. [19], pages 87–99.

[26] M.T. Rekveldt, W.G. Bouwman, Kraan W.H., O. Uca, S. Grigoriev, and R. Kreuger. Neutron spin echo, lecture notes in physics. In Mezei et al. [19], pages 100–115.

[27] J. Schelten and W. Schmatz. Multiple-scattering treatment for small-angle scattering problems. *Joural of Applied Crystallography,* 13:385–390, 1980.

[28] I. Sogami and N. Ise. *J. Chem. Phys.*, 81:6320–6332, 1984.

[29] D. M. E. Thies-Weesie, A. P. Philipse, G. Naegele, B. Mandl, and R. Klein. *J. Colloid Interface Sci.*, 176:43–54, 1995.

[30] G. J. Throop and R. J. Bearman. *Journal of Chemical Physics*, 42:2408–2411, 1965.

[31] O. Uca, W.G. Bouwman, and M.T. Rekveldt. Model calculations. *Journal of Applied Crystallography*, 36:109–116, 2003.

[32] Léon van Hove. Correlations in space and time and born approximation scattering in systems of interacting particles. *Physical Review*, 95:249–262, 1954.

[33] E. J. Verwey and J. Th. Overbeek. *Theory of the Stability og Lyophobic Colloids*. Elsevier, New York, 1948.

[34] S. R. Williams, I. K. Snook, and W. van Megen. *Phys. Rev. E*, 64:021506, 2001.

[35] A. J. C. Wilson. *Proc. Roy. Soc. A*, 180:277–285, 1942.

[36] F. Zernike and J.A. Prins. *Z.Physik*, 41:184–194, 1927.

Acknowledgements

List of Publications

1. Timofei Krouglov, Ignatz M. de Schepper, Wim G. Bouwman and M. Theo Rekveldt.
   Real-space interpretation of spin-echo small-angle neutron scattering.
   Journal of Applied Crystallography, (2003), **36**, 117-124.

2. Timofei Krouglov, Wicher H. Kraan, Jeroen Plomp, M. Theo Rekveldt and Wim G. Bouwman.
   Spin-echo small-angle neutron scattering to study particle aggregates.
   Journal of Applied Crystallography, (2003), **36**, 816-819.

3. M.Th.Rekveldt, W.G.Bouwman, W.H.Kraan, T.V.Krouglov, J.Plomp.
   Larmor precession applications: magnetised foils as spin flippers in spin-echo SANS with varying wavelength.
   Physica B, (2003), **335**, 164-168.

4. W.H.Kraan, J.Plomp, T.V.Krouglov, W.G.Bouwman and M.Th.Rekveldt.
   Ferromagnetic foils as monochromatic π-flippers for application in spin-echo SANS.
   Physica B, (2003), **335**, 247-249.

5. T. Krouglov, W. G. Bouwman, J. Plomp, M. T. Rekveldt, G. J. Vroege, A. V. Petukhov and D. M. E. Thies-Weesie.
   Structural transitions of hard-sphere colloids studied by spin-echo small-angle neutron scattering.
   Journal of Applied Crystallography, (2003), **36**, 1417-1423.

6. Wim G. Bouwman, Timofei V. Krouglov, Jeroen Plomp, S.V. Grigoriev, W.H. Kraan and M. Theo Rekveldt.
   SESANS studies of colloid phase transitions, dairy products and polymer fibers.
   Physica B, (2004), **350**, 140-146.

7. Wim G. Bouwman, Wouter Stam, Timofei V. Krouglov, Jeroen Plomp, Serguei V. Grigoriev, Wicher H. Kraan, M. Theo Rekveldt.
   SESANS with a monochromatic beam or with time-of-flight applied on colloidal systems.
   NIM A, (2004), **529**, 16-21.

8. Timofey Kruglov, Wim G. Bouwman, Jeroen Plomp, M. Theo Rekveld, gert jan Vroege, Andrei V. Petukhov and Dominique M.E.Thies-Weesie.
   Structure of hard-sphere colloid observed in real space by Spin-echo Small-angle Neutron Scattering.
   Physica B, (2005),**357**, 452-455.

9. Timofey V. Kruglov, Wim G. Bouwman, Ignatz M. de Schepper, M. Theo Rekveldt.
   Application of Spin-echo Small-angle Neutron Scattering to study the structure of charged colloids.
   Physica B, (2005),**356**, 218-222.

10. Wim G. Bouwman, Timofey Kruglov, Jeroen Plomp, M. Theo Rekveldt.
    Spin-echo methods for SANS and neutron reflectometry.
    Physica B, (2005), **357**, 66-72.

11. F.M. Mulder, J. Plomp, H.G. Schimmel, T.V. Krouglov, W.G. Bouwman and M.T.Rekveldt.
    Spontaneous aligned domains of single walled nanotube bundles on μm length scales
    in preparation.

12. S.V.Grigoriev, M.Th.Rekveldt, T. Kruglov, W.H.Kraan, W.G. Bouwman.
    Spin Echo SANS for magnetic samples.
    in preparation.

13. Timofey Kruglov.
    Correlation function of the excluded volume.
    Journal of Applied Crystallography, (2005), in press.

14. Timofey Kruglov.
    Spin-Echo Small-Angle Neutron Scattering for dense systems of spheres.
    Journal of Applied Crystallography, (2005), in press.

15. Timofey Kruglov, Wim G. Bouwman and Jeroen Plomp.
    Correlation function of the effective excluded volume and its application to charged colloids studied by Spin-echo Small-angle Neutron Scattering.
    in preparation.

Curriculum Vitae

Timofey Vladislavovich Kruglov (Timofei V. Krouglov) was born on July 13, 1975 in Narva, Estonia. He graduated in June 1992 with a gold medal (cum laude) from the Narva's school N1 with advanced physics and math. During his scholar years he had participated in all levels of mathematical, physical and chemical olympiads up to the International Physics Olympiad in Helsinki, Finland, July 1992. In September 1992 he moved to Saint-Petersburg, Russia to pursue his study at Saint-Petersburg State University. There he obtained bachelor (1996) and master (1998) degrees in physics. His bachelor' project was devoted to the rotational viscosity of liquid crystals and master' project to the optical birefringence induced by the external electric field (Kerr effect) in solutions of polymers. In 1999 he began a PhD project devoted to the light scattering in confined liquid crystals at the University of Puerto Rico. He quit in 2001. In August 2001 he begins his PhD project "Spin-Echo Small-Angle Neutron Scattering applied to colloidal systems" at Interfacultair Reactor Instituut in Delft, Netherlands. The results of this research are presented in this thesis.